Inorganic Chemistry

Article

pubs.acs.org/IC

Spectroscopic Characterization of the Active $Fe^{III}Fe^{III}$ and $Fe^{III}Fe^{II}$ Forms of a Purple Acid Phosphatase Model System

Peter Comba,*[,†] Lawrence R. Gahan,[‡] Valeriu Mereacre,[§] Graeme R. Hanson,[∥] Annie K. Powell,[§] Gerhard Schenk,[‡,⊥] and Marta Zajaczkowski-Fischer[†]

[†]Universität Heidelberg, Anorganisch-Chemisches Institut, INF 270, D-69120 Heidelberg, Germany

[‡]School of Chemistry and Molecular Biosciences, The University of Queensland, Brisbane, Queensland 4072, Australia

[§]Institut für Anorganische Chemie, Karlsruher Institut für Technologie, Enesserstrasse 15, D-76131 Karlsruhe, Germany

[∥]Centre for Advanced Imaging, The University of Queensland, Brisbane, Queensland 4072, Australia

[⊥]Department of Chemistry, National University of Ireland, Maynooth, Co. Kildare, Ireland

Supporting Information

ABSTRACT: Two new dinucleating ligands (H_3L^2 and HL^3), derivatives of a well-known dinucleating ligand (HL^1) with two bis-picolylamine sites connected to a bridging phenolate, with hydrogen-bonding donor groups at two of the pyridine moieties were designed and synthesized. Design of these ligands suggests that they will lead to dinuclear complexes with potential to stabilize phosphoester substrates as monodentate rather than bridging ligands. We report the diferric complexes $[Fe^{III}_2(H_2L^2)(OH)]^{4+}$ and $[Fe^{III}_2(L^3)(OH)(OH_2)_2]^{4+}$, which have been characterized by spectrophotometric titrations, UV−vis, IR, NMR, EPR, and Mössbauer spectroscopy. The phosphatase activity of the diferric systems, in addition to the partially reduced heterovalent $[Fe^{III}Fe^{II}(L^3)(OH)(OH_2)_2]^{3+}$ complex, has been investigated, and the complexes are shown to catalytically hydrolyze the activated phosphodiester substrate BDNPP (bis-dinitrophenyl-phosphate) as well as the corresponding phosphomonoester substrate DNPP (dinitrophenylphosphate). The results indicate that indeed the secondary interactions lead to an increase of the phosphatase activity and to active phosphomonoesterase catalysts. Interestingly, the heterovalent form of the HL^3-based complex is more efficient than the diferric complex, and this is also discussed.

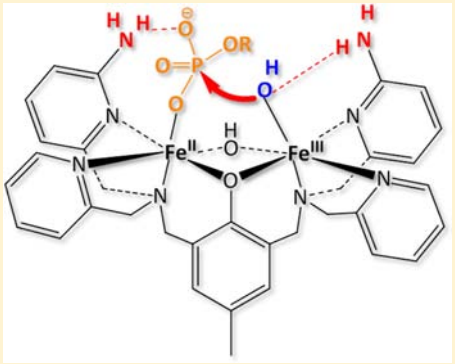

INTRODUCTION

Purple acid phosphatases (PAPs) catalyze the hydrolysis of phosphoester substrates in the pH range 3−8.[1−3] Structural, spectroscopic, mechanistic, and computational studies[4−7] of low molecular weight model compounds,[2,3,8] enzymes, and mutants have led to a thorough description of the mechanistic scenario of these and other metallohydrolases and to valuable ideas for applications in medicinal and environmental chemistry. While the PAP active site involves a dinuclear $Fe^{III}M^{II}$ metal center, where the divalent metal ion (M) is Fe^{II}, Zn^{II}, or Mn^{II}, catalytically competent substituted enzymes and model systems with Co^{II}, Cd^{II}, and Fe^{III} in the second site and catalytically competent $Mn^{III/II}Mn^{II}$ enzyme derivatives have also been described.[9−14] Interesting and of mechanistic relevance is the fact that while PAPs are able to hydrolyze phosphodiesters with significant activity, the biologically relevant hydrolysis of phosphomonoesters is generally not possible with model systems. In the only dinuclear PAP model compound able to hydrolyze phosphomonoesters, this was achieved with a diferric site in which the ligand platform provides hydrogen bonds to position the monoester substrate such that it coordinates monodentately and not as a bridging ligand.[15] We have also recently shown that a hydroxo-bridged dinuclear Cu^{II} cyclic peptide complex is capable of hydrolyzing both di- and monoester substrates.[16] These findings support the mechanistic proposal generally favored for PAP enzymes and model systems, whereby the substrate is hydrolyzed by nucleophilic attack of a terminal hydroxide.[17−20]

The phenolate-bridging ligand system $(L^1)^-$ (see Chart 1 for ligand structures) is known to hydrolyze phosphodiesters in its diferric form, but the heterovalent $Fe^{III}Fe^{II}$ form is also available and catalytically active.[21−23] We therefore hypothesized that a similar ligand system, which included substituents that provide hydrogen-bonding sites for the positioning of monoester substrates similar to the monoesterase model mentioned above, might lead to diferric as well as heterovalent complexes with monoesterase activity, producing the first structural and functional PAP monoesterase mimic. Models indicated that the ortho-substituted pyridine groups are ideally suited for hydrogen bonding to well-positioned substrates. These substituents should be moderately basic groups to mimic the histidine residues of PAP (the pK_a value of the amine group in 2-aminopyridine [pK_a = 6.8] is similar to that of 1*H*-imidazole

Received: June 25, 2012
Published: October 30, 2012

   dx.doi.org/10.1021/ic301347t | *Inorg. Chem.* 2012, 51, 12195−12209

Chart 1. Ligand Structures

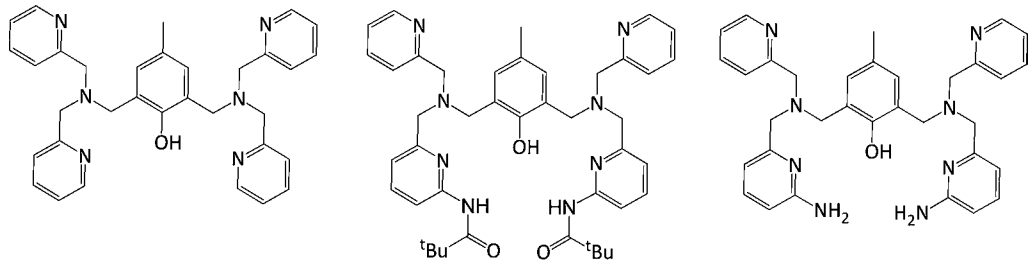

[pK_a = 7.0], and this has been used in other ligands to mimic the hydrogen bonding in enzyme active sites).[24−28] In order to maintain a small positive charge on the resulting complexes, only two of the four pyridine groups of HL^1 were functionalized.[29] Herein, we present the synthesis of the HL^3 ligand system, the corresponding amide intermediate H_3L^2 (see Chart 1 for ligand structures), and their iron complexes. The dinuclear $Fe^{III}Fe^{III/II}$ complexes are spectroscopically characterized, and their reactivity toward phosphoester hydrolysis examined.

RESULTS AND DISCUSSION

Ligand Synthesis. The two ligands H_3L^2 and HL^3 are derivatives of HL^1 (see Chart 1)[30] with a well-established preparative procedure.[30−32] Scheme 1 describes the synthesis of the two new ligands. Starting from commercially available 2-amino-6-methylpyridine, 2-formyl-6-pivaloylamidopyridine (**1**) is prepared according to published procedures.[33] The aldehyde is then reacted with 2-picolylamine to form the imine, which is reduced in situ with $NaBH_4$, to give the secondary amine (**2**) in quantitative yield. Ligand H_3L^2 is directly accessible in quantitative yield from **2** and 2,6-bis(chloromethyl)-*p*-cresol.[34,35] Attempts to obtain HL^3 from H_3L^2 by cleaving the protecting groups under reflux in 2 M HCl failed. It seems that these conditions are too harsh for the ligand backbone as only decomposition peaks were observed in electrospray ionization mass spectrometry (ESI-MS) of the crude reaction mixture. Therefore, an alternative approach was necessary; amine **2** was refluxed in 2 M HCl to deprotect the primary amine in quantitative yield. Subsequent reaction of the free amine **3** with 2,6-bis(chloromethyl)-*p*-cresol resulted in exclusive formation of HL^3 in 96% yield. As expected, the secondary amine functionality turned out to be the more active nucleophile and the primary amine protecting group was not necessary in this reaction. The overall yields for H_3L^2 and HL^3 are 25% (five steps) and 24% (six steps), respectively.

Scheme 1. Synthesis of Ligands H_3L^2 and HL^3 [a]

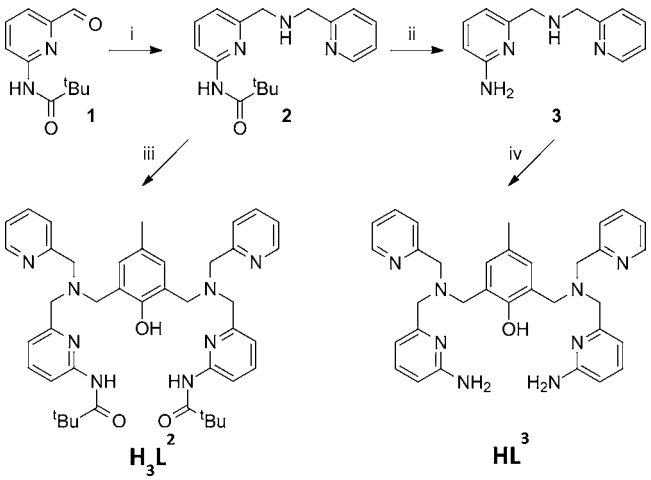

[a](i) Picolylamine, MeOH; $NaBH_4$; (ii) 2 M HCl; (iii and iv) 2,6-bis(chloromethyl)-*p*-cresol, CH_2Cl_2, THF, triethylamine.

In order to gain insight into the structural properties of the two new ligands, a conformational search was performed.[36−38] The most stable conformations of H_3L^2 and HL^3 are shown in Figure 1. For HL^3 various conformers were found within 10 kJ/mol, with the amine-appended pyridines either on one (cisoid) or on different sides (transoid) of the central phenol group. This is due to the high degree of flexibility of the donor groups. With H_3L^2, the lowest energy cisoid structure and its most stable transoid isomer are separated by 25 kJ/mol. Here, rotation around the C−C and C−N bonds of the methyl bridges is less favorable due to the more bulky amide groups. An additional effect derived from the structure of the lowest energy conformation in Figure 1 is that the amide groups are stabilized by intramolecular hydrogen bonds. This is only observed in the specific cisoid conformation shown.

Synthesis and Characterization of the Diferric Complexes. Solid diferric complexes of H_3L^2 and HL^3 were obtained by stirring the ligand with ferric perchlorate in hot methanol. Diffusion of diethyl ether into the corresponding complex solution precipitated $[Fe^{III}_2(H_2L^2)(OH)](ClO_4)_4$·MeOH. The complex of the amine-based ligand, $[Fe^{III}_2(L^3)(OH)(OH_2)_2](ClO_4)_4$·0.5MeCN·$Et_2O$, was obtained by diethyl ether diffusion into a solution of the complex in MeCN.[39] On the basis of the structure of similar complexes,[22,31,40,41] we assume that the coordination sphere of the Fe^{III} centers is completed by a μ-hydroxo bridge and two terminal water molecules in the HL^3-based complex. The amide oxygen atoms probably coordinate to the ferric ions in the H_3L^2-based complex,[41] and importantly, this clearly emerges from an analysis of the infrared spectra. This leaves a vacant site at each Fe^{III} center which is proposed to be filled by a bridging hydroxide (see Chart 2 for the proposed structures). These assignments are supported by an analysis of the infrared and the electronic spectra and redox properties discussed below.

Infrared (IR) spectra of the two diferric complexes are compared to the metal-free ligand spectra in Figure 2. The two peaks at 792 and 760 cm^{-1} in the spectrum of HL^3 (black curve in Figure 2b) are assigned to deformation vibrations of aromatic C−H groups (similar signals are observed for H_3L^2, black curve in Figure 2a). Absorptions at around 1500 and 1600 cm^{-1} are attributed to pyridine-group-derived C=N

dx.doi.org/10.1021/ic301347t | Inorg. Chem. 2012, 51, 12195−12209

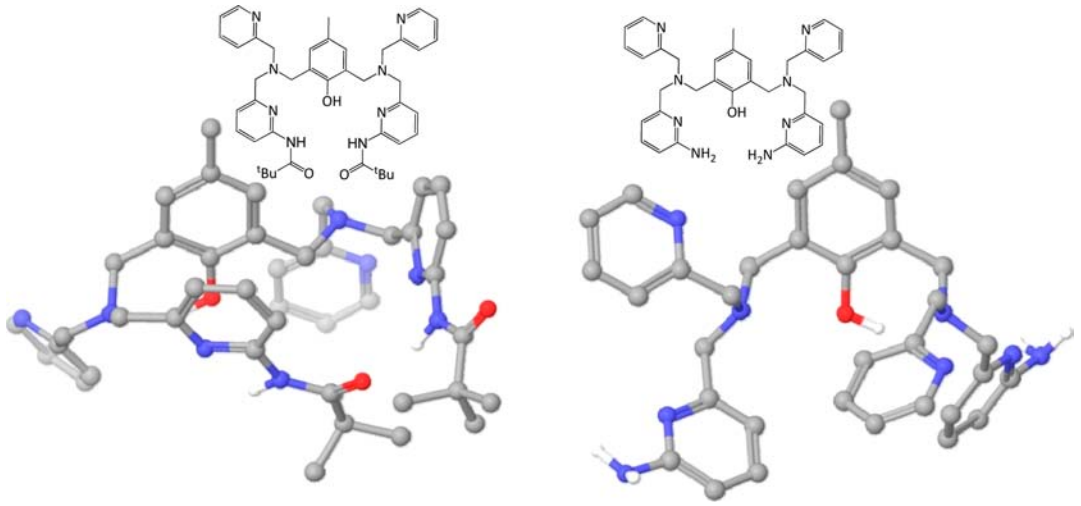

Figure 1. Computed structures of the lowest energy conformers of H_3L^2 (left) and HL^3 (right).

Chart 2. $[Fe^{III}_2(H_2L^2)(OH)](ClO_4)_4 \cdot MeOH$ (left) and $[Fe^{III}_2(L^3)(OH)(OH_2)_2](ClO_4)_4 \cdot 0.5MeCN \cdot Et_2O$ (right)

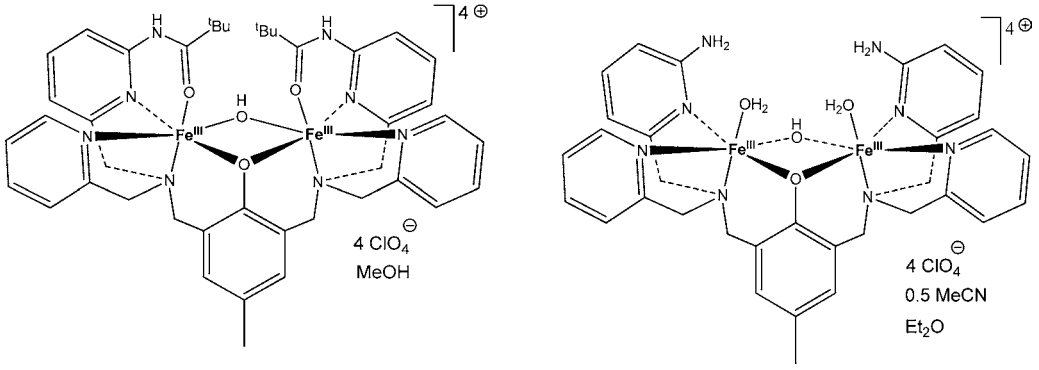

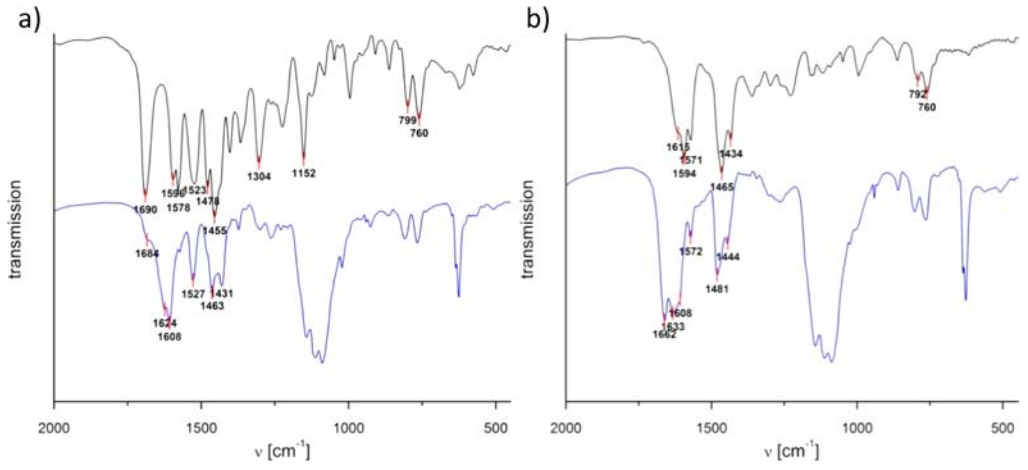

Figure 2. Infrared spectra of (a) ligand H_3L^2 (black line) and its complex $[Fe^{III}_2(H_2L^2)(OH)]^{4+}$ (blue line) and (b) ligand HL^3 (black line) and its complex $[Fe^{III}_2(L^3)(OH)(OH_2)_2]^{4+}$ (blue line).

valence vibrations; for HL^3, there are also NH_2-derived signals around 1600 cm^{-1}. A significant shift of the signals around 1600 and 1465 cm^{-1} toward higher energy is observed upon complexation of the amine derivative HL^3, viz. in the spectrum of $[Fe^{III}_2(L^3)(OH)(OH_2)_2]^{4+}$ (blue line in Figure 2b), and this is due to coordination of the pyridine groups. The position of the peak at 1571 cm^{-1} is almost unchanged and therefore assigned to an NH_2 vibration; some loss of intensity may be due to protonation of the amine group. Due to the amide substituents, the H_3L^2-based spectra are more complex (Figure 2a). The typical C═O stretching vibration is seen at 1690 cm^{-1}, the N−H bending terms at 1523 cm^{-1}, and the pyridine transitions around 1600 and 1500 cm^{-1}. Other intense absorptions at 1304 and 1152 cm^{-1} are assigned to O−H deformation and C−OH valence vibration (phenol group). Interestingly, the latter are not well resolved in the HL^3 spectrum, suggesting that in the amine-derived ligand HL^3 the phenol is at least partly deprotonated. The dominant C═O

dx.doi.org/10.1021/ic301347t | Inorg. Chem. 2012, 51, 12195−12209

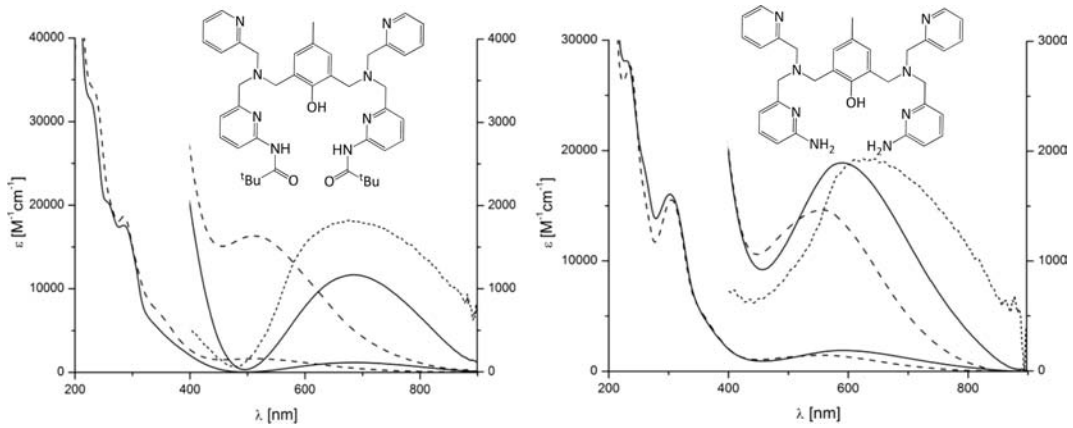

Figure 3. UV−vis spectra of $[Fe^{III}_2(H_2L^2)(OH)]^{4+}$ (left) and $[Fe^{III}_2(L^3)(OH)(OH_2)_2]^{4+}$ (right) in MeCN (solid line) and MeOH (dashed line) and in the solid state (dotted line).

vibration in the H_3L^2 spectrum at 1690 cm^{-1} is almost lost in the spectrum of $[Fe^{III}_2(H_2L^2)(OH)]^{4+}$ (Figure 2a) with the appearance of new bands at 1624 and 1608 cm^{-1}, which accounts for coordination of the carbonyl oxygens to Fe^{III}. In contrast, the amido NH vibration at 1523 cm^{-1} is retained, i.e., the amide part is still protonated in the complexes. The broad and intense signals around 1100 cm^{-1} as well as the sharp peak around 600 cm^{-1} in the complex spectra belong to perchlorate vibrations.

Electronic spectra of iron(III)−phenolate complexes and of diferric systems of this type of ligand in particular are generally dominated by phenolate to Fe^{III} ligand to metal charge transfer transitions (LMCT).[2,8,22,31,42] UV−vis spectra of $[Fe^{III}_2(H_2L^2)(OH)]^{4+}$ and $[Fe^{III}_2(L^3)(OH)(OH_2)_2]^{4+}$ were recorded in solution (MeCN and MeOH) and as isolated powders. Spectra of the two diferric complexes strongly depend on the medium (see Figure 3), specifically the absorption maxima of the phenolate-based LMCT transition (see also Table 1). The

Table 1. Phenolate-Based LMCT Transitions and Redox Potentials (Cyclic Voltammetry)[a] of $[Fe^{III}_2(H_2L^2)(OH)]^{4+}$ and $[Fe^{III}_2(L^3)(OH)(OH_2)_2]^{4+}$

	$[Fe^{III}_2(H_2L^2)(OH)]^{4+}$	$[Fe^{III}_2(L^3)(OH)(OH_2)_2]^{4+}$
λ_{MeCN} [nm] (ε [M^{-1} cm^{-1}])	685 (1946)	590 (2238)
λ_{MeOH} [nm] (ε [M^{-1} cm^{-1}])	517 (1630)	560 (1465)
λ_{solid} [nm]	681	630
$E_{1/2}$ vs $Fecp_2$ (SCE) [V]	0.022 (0.402)	−0.064 (0.316)

[a]In MeCN with 0.1 M NBu_4ClO_4 vs Ag/Ag^+; $E_{1/2}$ ($Fecp_2$) = 0.068 V.[44]

largest shift is observed with $[Fe^{III}_2(H_2L^2)(OH)]^{4+}$, where a change from MeCN to MeOH causes a hypsochromic shift of 168 nm. Compared to the solid state spectrum, the LMCT maximum in MeOH differs much more than in MeCN, indicating that the solid state structure may be retained in MeCN. In contrast, the significant changes to the LMCT wavelength maximum observed in MeOH, a harder donor solvent, are likely to be a consequence of ligand exchange through replacement of the hydroxide ligands by MeOH. The LMCT transitions of the two complexes are obviously also dependent on the protonation state, and candidates for relevant protonation equilibria are the bridging as well as the terminal hydroxide groups and the "hydrogen-bonding substituents" of the two ligand platforms.

Spectrophotometric pH Titrations. A spectrophotometric titration of $[Fe^{III}_2(H_2L^2)(OH)]^{4+}$ and $[Fe^{III}_2(L^3)(OH)(OH_2)_2]^{4+}$ was performed to analyze the pH dependence of the species distributions. The pH-dependent electronic spectra (see Figure 4a and 4b) were fitted with Specfit,[43] initially assuming three species in the pH range between 4.6 and 11, i.e., the diaqua, aqua−hydroxo, and dihydroxo complexes, analogous to published schemes for similar systems (see Scheme 2).[2] The proposed μ-hydroxo group is based on X-ray structures of analogous complexes[9] but is not proven in our systems. The resulting species distributions for three-species models are shown in Figure 4c and 4d, and Table 2 gives the associated pK_a values. Note that hydrogen bonding, induced by the substituents at two of the pyridine groups, may lead to selective stabilization of certain protonation steps, and this is visualized in a possible structure of $[Fe^{III}_2(L^3)(OH)(OH_2)_2]^{4+}$. Note however that the pK_a values of the coordinated water molecules and the dangling hydrogen-bonding groups are in a similar range (pK_a = 6.8 for 2-aminopyridine, the coordinated OH_2 groups have generally pK_a values between approximately 5 and 9). Therefore, there is no unambiguous assignment of the observed pK_a values.

With the protonatable pendent groups of H_3L^2 and HL^3, it appears that more than three species might be involved in the solutions studied by spectrophotometric titrations, i.e., protonation/deprotonation equilibria due to the ammonium and amide side chains might be of importance in modeling the titration data. With HL^3, the pyridine-appended amines are protonated at low pH and therefore do not form hydrogen bonds to the Fe^{III}−OH_2 groups. Deprotonation of either one of these ammonium groups or a coordinated OH_2 ligand will lead to the possibility of hydrogen bonds, which may significantly stabilize such species. Similar effects may influence the corresponding solution chemistry of the amide-derived ligand complexes, that is, the two possible protonation sites of complexes of H_3L^2 and HL^3 suggested that more than the three species shown in Scheme 2 might be required to accurately model the spectrophotometric data. Therefore, we also used four-species models for the data-fitting procedures, and these are also presented in Table 2. From the standard deviations of the corresponding fits it appears that the three-species model is appropriate for the H_3L^2-based system, while for the HL^3-based diiron(III) complex a four-species model seems to be

dx.doi.org/10.1021/ic301347t | Inorg. Chem. 2012, 51, 12195−12209

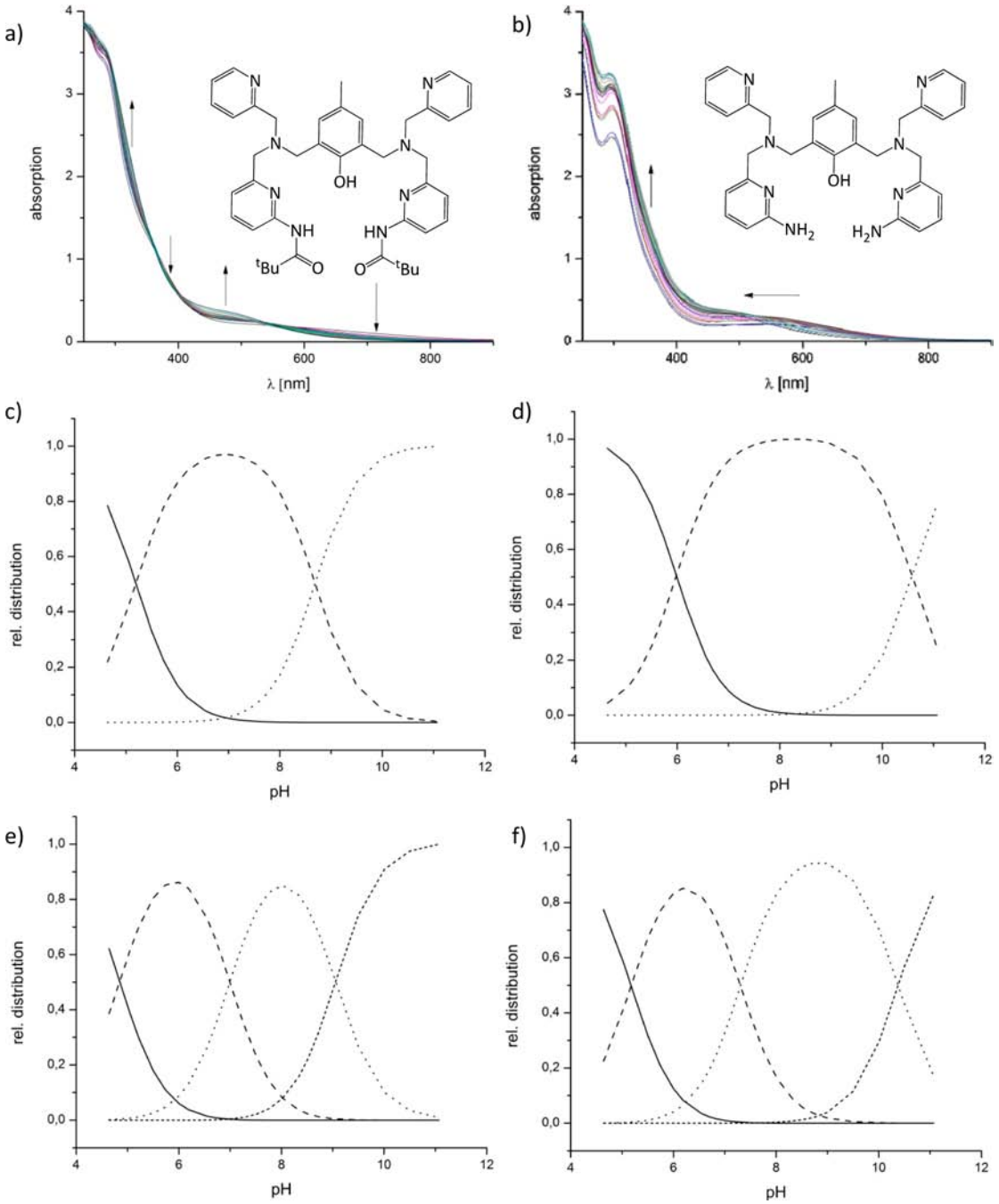

Figure 4. Spectrophotometric titration of (a) $[Fe^{III}_2(H_2L^2)(OH)]^{4+}$ and (b) $[Fe^{III}_2(L^3)(OH)(OH_2)_2]^{4+}$ in MeOH/buffer between pH 4.6 and 11 (arrows indicate the changes from low to high pH) and the resulting species distribution (see text) for a three- and four-species model, respectively, for $[Fe^{III}_2(H_2L^2)(OH)]^{4+}$ (c and e) and $[Fe^{III}_2(L^3)(OH)(OH_2)_2]^{4+}$ (d and f). Relevant pK_a values are given in Table 2 and may also be compared with those from the kinetic analysis in Tables 7 and 8.

preferable. However, this choice is to a large extent arbitrary. It therefore is important to note that two pK_a values for each complex are to a large extent independent of the model used (i.e., within the error limit identical) and are in the range expected for dinuclear iron(III)−aqua complexes, i.e., around $pK_a^I = 5$ and $pK_a^{II} = 9$. The important information is that both complexes are expected to operate as phosphatases in a pH range similar to that of the natural systems and of the well-established L^1-based catalyst, and the L^3-based species is expected to operate in a significantly broader pH range than both the unsubstituted and the amide-based systems. This is also obvious from the species distributions (Figure 4) and will be discussed in the context of the kinetic data below.

Redox Properties of $[Fe^{III}_2(H_2L^2)(OH)]^{4+}$ and $[Fe^{III}_2(L^3)(OH)(OH_2)_2]^{4+}$. The redox properties of $[Fe^{III}_2(H_2L^2)(OH)]^{4+}$ and $[Fe^{III}_2(L^3)(OH)(OH_2)_2]^{4+}$ were examined by cyclic voltammetry, and data are summarized in Table 1 (between 50 and 800 mV/s the potentials are independent of the scan speed).[44] Potentials are assigned to $Fe^{III}_2/Fe^{III}Fe^{II}$ couples and are in the range of but slightly lower than reported values of similar tetrakis-pyridyl ligands.[2,8,22,31,42] This explains why our complexes are highly stable under aerobic conditions in their homovalent diferric state. However, a reduction under

dx.doi.org/10.1021/ic301347t | Inorg. Chem. 2012, 51, 12195−12209

Scheme 2. Protonation Equilibria of $[Fe^{III}_2(H_2L^2)(OH)]^{4+}$ and $[Fe^{III}_2(L^3)(OH)(OH_2)_2]^{4+}$ in a Three-Species Model[a]

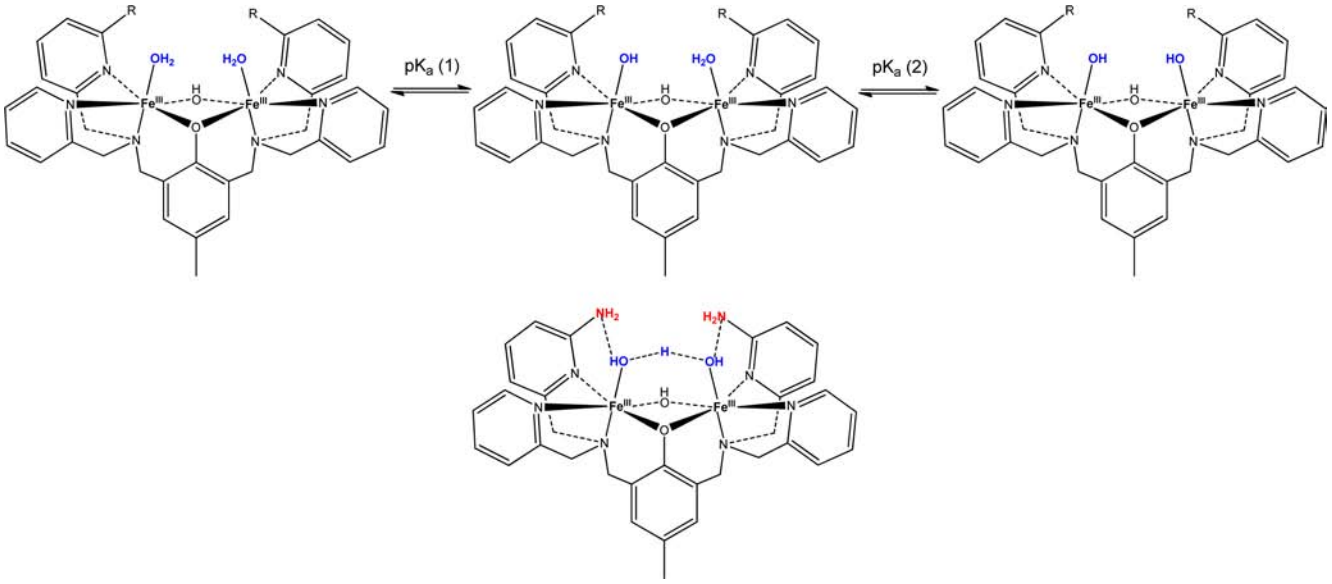

[a]Also shown is a possible doubly deprotonated species of $[Fe^{III}_2(L^3)(OH)(OH_2)_2]^{4+}$, indicating that the amine substituents may lead to a stabilization of certain species via hydrogen bonding, see text.

Table 2. Fitted pK_a Values from Spectrophotometric Titrations of $[Fe^{III}_2(H_2L^2)(OH)]^{4+}$ and $[Fe^{III}_2(L^3)(OH)(OH_2)_2]^{4+}$

$[Fe^{III}_2(H_2L^2)(OH)]^{4+}$		$[Fe^{III}_2(L^3)(OH)(OH_2)_2]^{4+}$	
3 species	4 species	3 species	4 species
5.19 ± 0.17	4.85 ± 0.22	5.98 ± 0.12	5.18 ± 0.19
	6.99 ± 0.28		7.31 ± 0.25
8.69 ± 0.14	9.05 ± 0.19	10.57 ± 0.57	10.38 ± 0.35

anaerobic conditions to the heterovalent $Fe^{III}Fe^{II}$ complexes produces stable compounds, and this is described in the next section.

Synthesis and Characterization of Heterovalent Complexes. The heterovalent $Fe^{III}Fe^{II}$ complexes of H_3L^2 and HL^3, $[Fe^{III}Fe^{II}(H_2L^2)(OH)]^{3+}$, and $[Fe^{III}Fe^{II}(L^3)(OH)(OH_2)_2]^{3+}$ [39] were obtained from bulk electrolysis (one-electron reduction) of $[Fe^{III}_2(H_2L^2)(OH)]^{4+}$ and $[Fe^{III}_2(L^3)(OH)(OH_2)_2]^{4+}$. The resulting solutions were analyzed by UV−vis spectroscopy in comparison with the corresponding spectra of the diferric complexes and for the H_3L^2-based system also with electron paramagnetic resonance (EPR) and ^{57}Fe Mössbauer spectroscopy. The most prominent change in the UV−vis spectra (see Figure 5 and Table 3) is a decrease in intensity to approximately 50% of the phenolate-based LMCT band around 600 nm. With $[Fe^{III}_2(H_2L^2)(OH)]^{4+}$, the reduced

Table 3. Phenolate-Based LMCT Transitions of $[Fe^{III}_2(H_2L^2)(OH)]^{4+}$, $[Fe^{III}_2(L^3)(OH)(OH_2)_2]^{4+}$, $[Fe^{III}Fe^{II}(H_2L^2)(OH)]^{3+}$, and $[Fe^{III}Fe^{II}(L^3)(OH)(OH_2)_2]^{3+}$

	Fe^{III}_2/L^2	$Fe^{III}Fe^{II}/L^2$ (red)	Fe^{III}_2/L^2 (reox)	Fe^{III}_2/L^3	$[Fe^{III}Fe^{II}/L^3$ (red)
λ_{MeCN} [nm]	685	600 (sh)	619	590	590
ε [M^{-1} cm^{-1}]	1946	852	1931	2238	1031

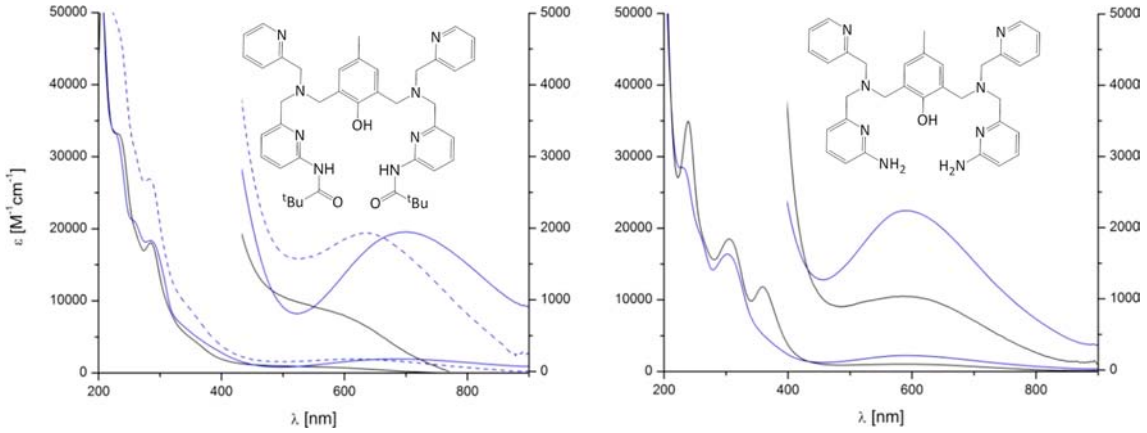

Figure 5. UV−vis spectra of the bulk-electrolysis experiments [MeCN, 0.1 M $(NBu_4)(ClO_4)$] of (a) the amide-ligand-based system [(blue curve) $[Fe^{III}_2(H_2L^2)(OH)]^{4+}$; (black curve) $[Fe^{III}Fe^{II}(H_2L^2)(OH)]^{3+}$; (black curve) $[Fe^{III}_2(H_2L^2)(OH)]^{4+}$ (see text)] and (b) the amine-ligand-based system [(blue curve) $[Fe^{III}_2(L^3)(OH)(OH_2)_2]^{4+}$; (black curve($[Fe^{III}Fe^{II}(L^3)(OH)(OH_2)_2]^{3+}$].

dx.doi.org/10.1021/ic301347t | Inorg. Chem. 2012, 51, 12195−12209

solution was reoxidized by applying a potential of +200 mV for 30 min (dashed blue line in Figure 5a). The intensity of the LMCT transition is restored, suggesting reformation of a diferric complex, but the absorption maximum is significantly shifted to higher energy, i.e., the diferric complex thus formed differs from the initial complex $[Fe^{III}_2(H_2L^2)(OH)]^{4+}$. With the amine-based ligand system, the electrochemically produced heterovalent complex $[Fe^{III}Fe^{II}(L^3)(OH)(OH_2)_2]^{3+}$ was exposed to air, and UV−vis spectrophotometry indicated that it is not spontaneously reoxidized to the diferric state (see Supporting Information; with the amide-based ligand this is even less likely due to the lower reduction potential).

The heterovalent state of $[Fe^{III}Fe^{II}(H_2L^2)(OH)]^{3+}$ was confirmed by Mössbauer spectroscopy: a ^{57}Fe-enriched sample of $[Fe^{III}_2(H_2L^2)(OH)]^{4+}$ was prepared in situ from H_3L^2 and $(NEt_4)[^{57}FeCl_4]$, followed by bulk electrolysis.[45] In this experiment, the reduction to the heterovalent state was incomplete (see Experimental Section; only around 30% yield of the $Fe^{III}Fe^{II}$ form). However, the Mössbauer spectrum clearly shows signals of both ferric and ferrous species (see Figure 6 and Table 4). At 30 K, two doublets are found: the

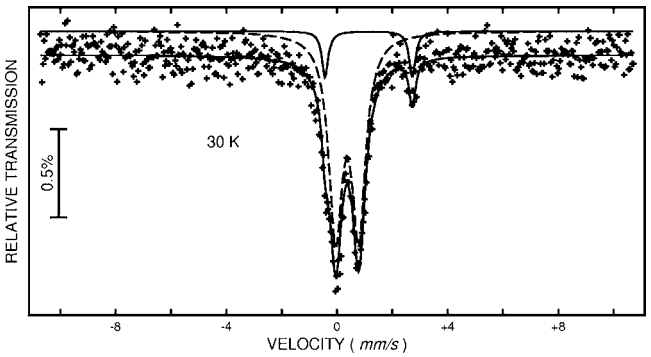

Figure 6. Mössbauer spectrum of $[Fe^{III}Fe^{II}(H_2L^2)(OH)]^{3+}$ at 30 K (for parameters see Table 3).

Table 4. Simulated Mössbauer Parameters of $[^{57}Fe^{III}\,^{57}Fe^{II}(H_2L^2)(OH)]^{3+}$

assignment	δ^a, mm/s	ΔE_Q, mm/s	Γ, mm/s	area, %
Fe^{II}	1.25(1)	3.15(3)	0.27(8)	9.9
Fe^{III}	0.476(6)	0.84(1)	0.59(2)	90.1

[a]Isomer shifts are given relative to α-Fe at room temperature.

first, with an isomer shift δ = 1.25(1) mm/s (relative to α-iron) and a quadrupole splitting of 3.15(3) mm/s, is typical for Fe^{II} ions in the high-spin state; the second, with an isomer shift δ = 0.47(6) mm/s and a quadrupole splitting of 0.84(1) mm/s, is typical for Fe^{III} ions in the high-spin state. The ratio of the doublet areas is ∼1: 9, which is in acceptable agreement with the ∼30% yield of the $Fe^{III}Fe^{II}$ form after electrolysis.

The EPR spectrum of the diferric complex $[Fe^{III}_2(H_2L^2)(OH)]^{4+}$ (MeCN/aqueous buffer, 1.7 K, see Figure 7) has a weak signal with resonances at g_{eff} = 9.109, 7.109, and 4.238, typical of an orthorhombically distorted high-spin Fe^{III} center and most probably arises from a small impurity of a monomeric Fe^{III} species. The absence of an EPR spectrum from the dinuclear Fe^{III} complex at low temperature was expected on the basis of solution magnetic moments (determined by the Evans-NMR method at 298 K),[46] which indicate a high-spin S = 5/2 configuration for the mononuclear Fe^{III} complex, and a room-

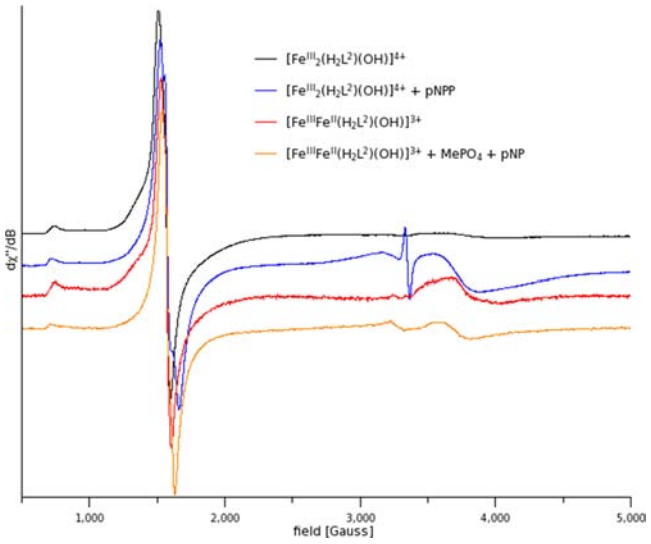

Figure 7. EPR spectra (MeCN, 1.7 K, 9.6 GHz) of $[Fe^{III}_2(H_2L^2)(OH)]^{4+}$ (black), $[Fe^{III}_2(H_2L^2)(OH)]^{4+}$ with pNPP (blue), $[Fe^{III}Fe^{II}(H_2L^2)(OH)]^{3+}$ (red), and $[Fe_2(H_2L^2)(OH)_2]^{3+}$ with methyl phosphate and *p*-nitrophenol (orange).

temperature magnetic moment, typical for an S = 2 thermally populated spin state of an antiferromagnetically coupled dinuclear Fe^{III} complex, where the exchange coupling is moderately large (see below). The electrochemically produced heterovalent complex $[Fe^{III}Fe^{II}(H_2L^2)(OH)]^{3+}$ gives a more complex EPR spectrum with additional resonances around g_{eff} = 4.3 and 2 (see Figures 7 and 8).

Interestingly, reaction of the diferric complexes $[Fe^{III}_2(H_2L^2)(OH)]^{4+}$ and $[Fe^{III}_2(L^3)(OH)(OH_2)_2]^{4+}$ with the largely hydrolytically stable phosphomonoester *p*-nitrophenyl phosphate (pNPP) leads to very similar EPR signals as observed for the heterovalent complex $[Fe^{III}Fe^{II}(H_2L^2)(OH)]^{3+}$ (see Figures 7 and 8). We assumed that a minor amount of *p*-nitrophenol, resulting from partial hydrolysis of pNPP, might be the one-electron reductant, resulting in a relatively stable phenoxy radical. However, when *p*-nitrophenol was added to a solution of $[Fe^{III}_2(H_2L^2)(OH)]^{4+}$, no radical signals were detected by EPR spectroscopy. In PAP it was observed that phosphate lowers the redox potential of the iron in the second site by as much as 50%.[47] Therefore, we assume that the coordinated pNPP reduces the redox potential of the complex and facilitates partial reduction of the diferric species. Indeed, when $[Fe^{III}_2(H_2L^2)(OH)]^{4+}$ is allowed to react with methyl phosphate (stable against hydrolysis under the conditions of our experiments) and subsequently with *p*-nitrophenol (pNP), an EPR spectrum very similar to that of $[Fe^{III}_2(H_2L^2)(OH)]^{4+}$ with pNPP was observed (Figure 7).

Variable-temperature experiments (results not shown) indicate weak exchange coupling for these complexes as the intensity of all resonances around g_{eff} = 4.3 and 2 decreases as the temperature is increased from 1.5 K. Computer simulation of the EPR spectrum of $[Fe^{III}_2(L^3)(OH)(OH_2)_2]^{4+}$ with pNPP (Figure 8b) with the spin Hamiltonian parameters in Table 5 produces a satisfactory fit.[48] The resonances around g_{eff} = 12.0 and 4.3 arise from transitions within the $|\pm 3/2\rangle$ doublets of thermally populated S_{tot} = 3/2 and 5/2 doublets of a weakly antiferromagnetically coupled dinuclear $Fe^{III}Fe^{II}$ complex. While the computer simulation of the resonances around g_{eff} ≈ 2 in the EPR spectrum of a solution containing $[Fe^{III}_2$

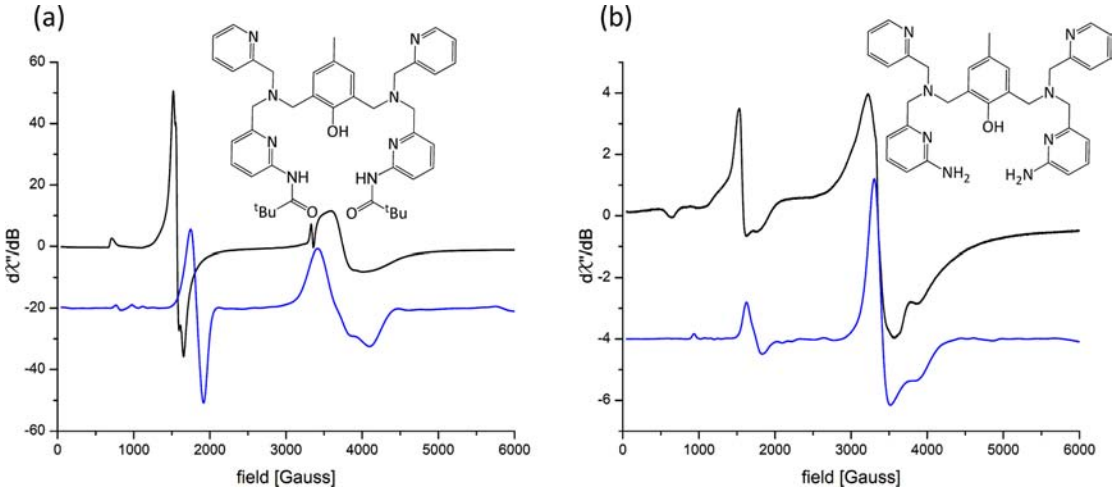

Figure 8. Experimental (black) and simulated (blue; spin Hamiltonian parameters are given in Table 4) X-band EPR spectra of (a) $[Fe^{III}_2(H_2L^2)(OH)]^{4+}$ with pNPP and (b) $[Fe^{III}_2(L^3)(OH)(OH_2)_2]^{4+}$ with pNPP in MeCN/buffer pH 5 at 0.5 and 10 mM complex and substrate concentration, respectivly; spectra were measured at (a) 1.5 K and 9.37863 GHz and (b) 1.6 K and 9.379757 GHz.

Table 5. Calculated (DFT, see Experimental Section) and Simulated Spin Hamiltonian Parameters (see Figure 6, MoSophe[48]) of $[Fe^{III}_2(H_2L^2)(OH)]^{4+}$ with pNPP and (b) $[Fe^{III}_2(L^3)(OH)(OH_2)_2]^{4+}$ with pNPP

	$[Fe^{III}_2(H_2L^2)(OH)]^{4+}$ + pNPP[a]		$[Fe^{III}_2(L^3)(OH)(OH_2)_2]^{4+}$ + pNPP[b]	
parameter	calcd	sim.	calcd	sim.
g_{iso} Fe^{III}	2.07	2.08	2.07	2.09
g_{iso} Fe^{II}	2.10	2.14	2.24	2.15
D_1 Fe^{III} [cm^{-1}]	1.161	0.021	−1.091	0.0012
E/D Fe^{III}	0.118	0.002	0.095	0.000
D_2 Fe^{II} [cm^{-1}]	1.262	1.002	−2.327	0.82
E/D Fe^{II}	*c*	0.180	*c*	0.045
d (Fe−Fe) [Å]	3.904	3.900	4.012	3.900
J_{iso} [cm^{-1}][d]	*c*	−1.84	*c*	−2.06

[a] *D* tensor orientation $\alpha/\beta/\gamma$ [°] = 10/−50/0 for Fe^{III} and −10/50/0 for Fe^{II}. [b] *D* tensor orientation $\alpha/\beta/\gamma$ [°] = 20/−60/0 for Fe^{III} and −20/60/0 for Fe^{II}. [c] Calculated values are not available. [d] $H = -2J_{iso}\mathbf{S}_1\cdot\mathbf{S}_2$.

$H_2L^2)(OH)]^{4+}$ and pNPP (Figure 8a) agree well with experiment, those around $g_{eff} \approx 4.3$ do not, presumably a consequence of an underestimate of the zero-field splitting and/or exchange coupling and their overlap with resonances from $[Fe^{III}_2\ H_2L^2)(OH)]^{4+}$.

In the amide-based system $[Fe^{III}Fe^{II}(H_2L^2)(OH)]^{3+}$ an additional sharp resonance at $g = 2.00649$ is observed, and this is assigned to a free radical species. A room-temperature EPR spectrum of the same sample (Figure 9) shows a complex radical signal. Computer simulation[49] reveals that the radical is not the *p*-nitrophenoxy radical but that the unpaired electron is located on the ligand backbone (see Figure 9 for the experimental and simulated spectra, the ligand structure, and relevant parameters). It is likely that the electron is transferred from initially formed *p*-nitrophenoxide to the ligand and stabilized there. In order to establish whether the unpaired electron was present on the ligand of the intact dinuclear $[Fe_2^{III}(H_2L^2)(OH)]^{4+}$ complex or associated with a decomposition product (loss of Fe^{III} ions) we also measured the EPR

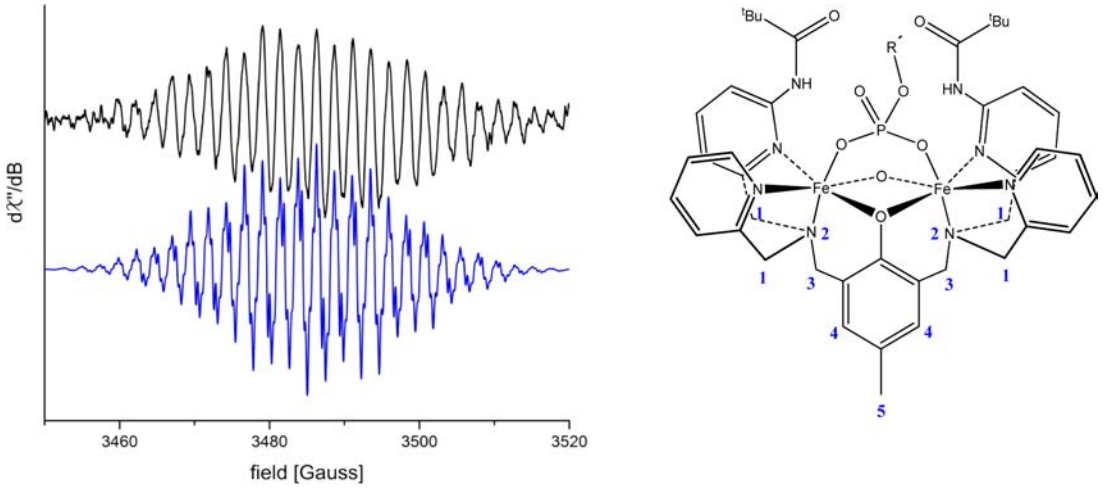

Figure 9. Experimental (black) and simulated (blue) X-band EPR spectrum of the radical generated by $[Fe^{III}_2(H_2L^2)(OH)]^{4+}$ with pNPP in MeCN/buffer pH 5 (0.5 mM $[Fe^{III}_2(H_2L^2)(OH)]^{4+}$, 10 mM pNPP) measured at 9.788782 GHz, 298 K and 1.0 G modulation amplitude. Spin Hamiltonian parameters are as follows: $g = 2.00649$, *A* (^{1}H) 1.26 (8×, CH_2 ***1***), *A* (^{14}N) 20.22 (2×, *N* ***2***), *A* (^{1}H) 20.22 (4×, CH_2 ***3***), *A* (^{1}H) 6.74 (2×, *CH* ***4***), *A* (^{1}H) 6.74 (3×, CH_3 ***5***). Units are MHz.

dx.doi.org/10.1021/ic301347t | *Inorg. Chem.* 2012, 51, 12195−12209

spectrum of the ^{57}Fe-enriched complex to see whether ^{57}Fe hyperfine coupling could be resolved. While the signal-to-noise ratio of the room-temperature EPR spectrum of a solution containing $[^{57}Fe_2^{III}(H_2L^2)(OH)]^{4+}$ and pNPP (see Supporting Information) was not as high as the spectrum for naturally abundant Fe (Figure 9), it is clear from the additional splitting that the unpaired electron is located on the ligand of the intact complex.[50]

Mössbauer spectra of $[^{57}Fe^{III}_2(H_2L^2)(OH)]^{4+}$ after addition of pNPP do not show any signals for Fe^{II}. This is not entirely unexpected and indicates that the redox process discussed above only leads to a very small amount of the side products, i.e., it probably is not mechanistically relevant in the diferric system.

The magnetic properties of $[Fe^{III}_2(H_2L^2)(OH)]^{4+}$ and $[Fe^{III}_2(L^3)(OH)(OH_2)_2]^{4+}$ were examined by Evans-NMR. Methanolic solutions of ligand and tetrachloroferrate were mixed in 1:1 or 1:2 ratios. The results of the magnetic studies are summarized in Table 6. The 1:1 mixtures with both ligands, HL^2 and H_3L^3, have significantly larger μ_{eff} values than the 1:2 samples. This is consistent with uncoupled monomeric high-spin Fe^{III} complexes, although the experimental values are higher than the expected spin-only value of 5.92. This is a usual observation, as contributions of spin−orbit coupling lead to higher values. Nevertheless, addition of base leads to a decrease of μ_{eff} which can be explained by formation of at least a small fraction of dinuclear complexes. With 2 equiv of Fe^{III}, μ_{eff} takes values that correspond to dinuclear systems with relatively strong coupling. The expected spin state of $S = 2$ is the closest value corresponding to the experiment. On the basis of known complexes of this type, J_{iso} ($H = -2J_{iso}\mathbf{S}_1.\mathbf{S}_2$) values between −5 and −15 cm^{-1} should be expected,[51,52] originating from moderate coupling through the phenoxide bridge. This value would however lead to a larger μ_{eff}. Spin states of $S = 3$ or 4 can be populated at room temperature in this case. Thus, additional bridging ligands, like μ-oxo, might be present to increase the coupling.[53] Assuming that no unbound Fe^{III} is present in the sample, exchange coupling constants of larger than 30 cm^{-1} can be expected for both complexes.

Table 6. Results of Evans-NMR Experiments of the Mono- and Dinuclear Fe^{III} Complexes of H_3L^2 and HL^3

sample	exp. μ_{eff} [B.M.] per complex unit	expected spin state S	calcd μ_{eff} [B.M.] for expected spin state
H_3L^2 + 1Fe^{III}	6.52	5/2	5.92
H_3L^2 + 1Fe^{III} + 1NEt_3	6.03	5/2	5.92
H_3L^2 + 2Fe^{III}	4.63	2	4.90
H_3L^2 + 2Fe^{III} + 2NEt_3	4.24	2	4.90
HL^3 + 1Fe^{III}	6.77	5/2	5.92
HL^3 + 1Fe^{III} + 1NEt_3	6.16	5/2	5.92
HL^3 + 2Fe^{III}	4.73	2	4.90
HL^3 + 2Fe^{III} + 2NEt_3	4.24	2	4.90

Phosphatase Activity of $[Fe^{III}_2(H_2L^2)(OH)]^{4+}$, $[Fe^{III}_2(L^3)(OH)(OH_2)_2]^{4+}$, and $[Fe^{III}Fe^{II}(L^3)(OH)(OH_2)_2]^{3+}$. The activity of the amide- and amine-based ligand diferric complexes $[Fe^{III}_2(H_2L^2)(OH)]^{4+}$ and $[Fe^{III}_2(L^3)(OH)(OH_2)_2]^{4+}$ and the amine ligand-based heterovalent complex $[Fe^{III}Fe^{II}(H_2L^3)(OH)(OH_2)_2]^{3+}$ toward hydrolysis of the activated phosphoester substrates bis(2,4-dinitrophenyl)phosphate (BDNPP, diester)[54] and 2,4-dinitrophenylphosphate (DNPP, monoester)[55] were measured with a published spectrophotometric assay.[12,15,42,56−59] For comparison, we also tested the activity of the diferric HL^1-based complex toward hydrolysis of BDNPP, as this has not been reported so far. The observed rate laws are all described by a mechanism characteristic of Michaelis−Menten-type behavior; as the substrate concentration is increased the reaction order gradually changes from 1 to 0.[60] According to this mechanism the initial rapid formation of a complex between the catalytic model and the substrate is followed by the hydrolytic step with a rate of k_{cat}. The observed hyperbolic dependence of the initial rate on the concentration of the substrate is described by eq 1. Selected data are shown in Figure 10 (the entire series of plots is given as Supporting Information), and data are summarized in Tables 7 and 8. Similar data were previously obtained for other PAP mimics, indicating that all these systems employ a similar mechanistic strategy.[9,10,12,40,42,61]

$$v = \frac{v_{max}[S]_0}{K_m + [S]_0} \quad (1)$$

From an analysis of the kinetic data (see Figure 10 and Supporting Information as well as eqs 1−3 below)[62] two limiting pK_a values are evident (see Table 7). The corresponding protonation equilibria are assigned to the two water molecules coordinated terminally to the two metal ions (see Scheme 2). Similar values were obtained for the HL^1- and H_3L^2-based systems, but pK_a(II) is significantly higher for the HL^3-based complexes. This agrees qualitatively with the interpretation of the spectrophotometric titrations discussed above (Table 2, Figure 4; overlay plots are given as Supporting Information): The fact that a three-species model is appropriate for the amide-based system $[Fe^{III}_2(H_2L^2)(OH)]^{4+}$ and a four-species model is more appropriate for the amine-based catalyst $[Fe^{III}_2(L^3)(OH)(OH_2)_2]^{4+}$ might imply that the aqua−hydroxo species in the latter system is stabilized by hydrogen bonding (pK_a(3) in Table 2 corresponds to pK_a(II) of the kinetic analysis; see also Scheme 2). A similar effect is observed in the kinetic analysis of the heterovalent complex (Table 7). Importantly, the two new systems based on H_3L^2 and HL^3 have, with the phosphodiester BDNPP, similar catalytic efficiencies compared with the HL^1-based diferric system (k_{cat}/K_M in Table 7), i.e., the higher substrate binding constant K_M (factor of approximately 4, probably due to hydrogen bonding) is compensated by faster hydrolysis rates k_{cat}. Interestingly and not unexpectedly, the catalytic efficiency of the heterovalent HL^3-based catalyst is more than 5-fold increased with respect to the corresponding diferric system (k_{cat}/K_M in Table 7), and this is due to a smaller substrate binding constant (K_M, Fe^{II} vs Fe^{III}) and a faster rate.

The main feature, however, is the catalytic hydrolysis of the phosphomonoester substrate DNPP (Figure 10 and Table 8). This biologically important reaction was so far only observed with one low-molecular-weight model system, where it was shown to be induced by second coordination sphere hydrogen bonding.[15] Ligands H_3L^2 and HL^3 were designed to also prevent coordination of phosphomonoesters as bridging ligands, and the observed reactivity (Table 8) indicates that indeed this is the case, i.e., the reactivities are significant, and in terms of the catalytic efficiencies (i.e., the k_{cat}/K_M ratios) even exceeding those of the phosphodiester substrates. As in the

dx.doi.org/10.1021/ic301347t | Inorg. Chem. 2012, 51, 12195−12209

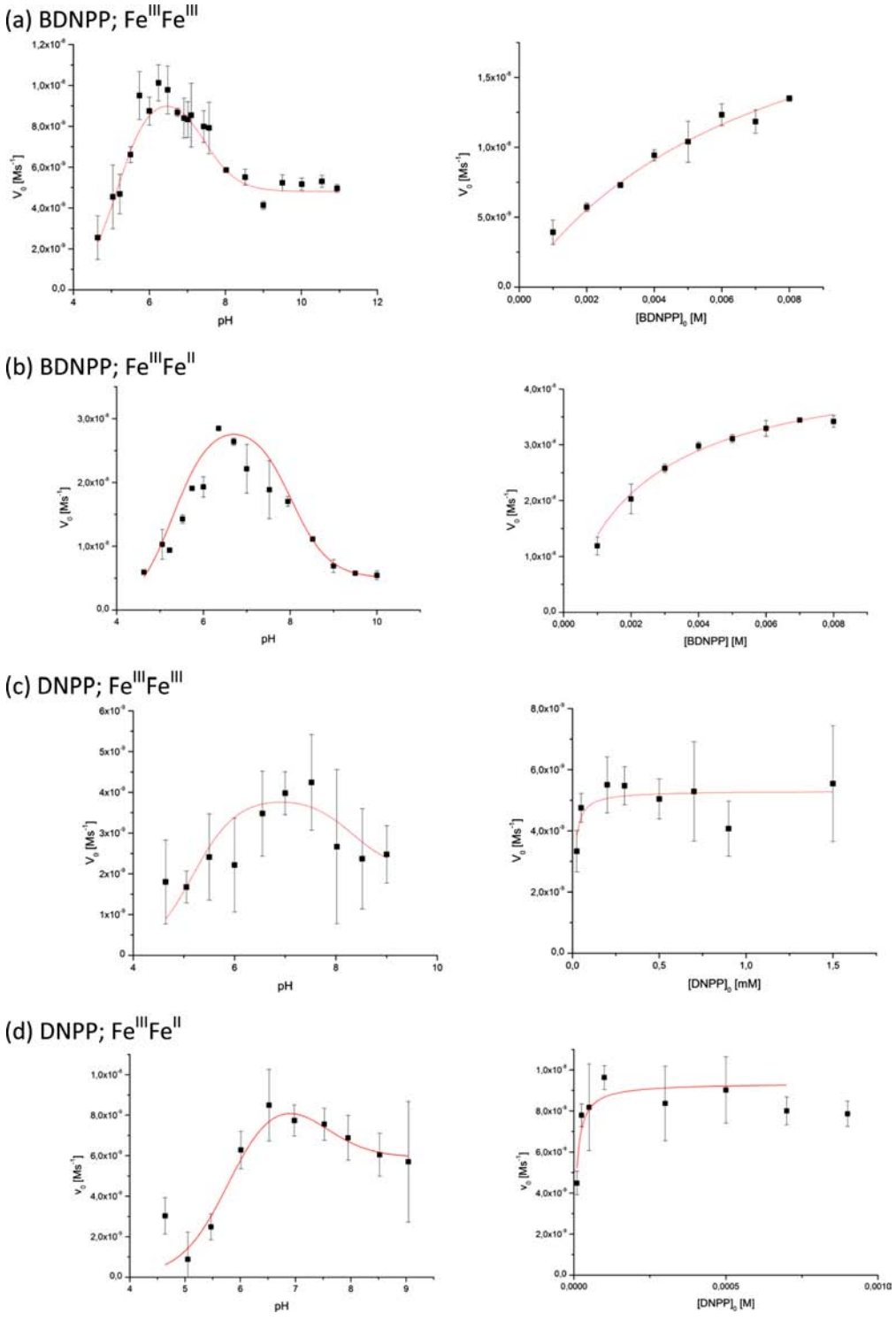

Figure 10. BDNPP (a and b) and DNPP hydrolysis (c and d); (left) pH profiles, (right) Michaelis–Menten diagrams of (a and c) $[Fe^{III}_2(L^3)(OH)(OH_2)_2]^{4+}$ and (b and d) $[Fe^{III}Fe^{II}(L^3)(OH)(OH_2)_2]^{3+}$ (black squares are experimental data, red lines are fits using eqs 1 and 2 for pH profiles and Michaelis–Menten diagrams, respectively).

recently published example with a cyclam-based platform,[15] this further confirms the assumed mechanism, with a terminal hydroxo ligand attacking the monodentatedly bound phosphoester.[2,3,63] More importantly, we are able to show for the first time that an $Fe^{III}M^{II}$ system, i.e., $[Fe^{III}Fe^{II}(L^3)(OH)(OH_2)_2]^{3+}$, is able to hydrolyze the phosphomonoester model substrate DNPP (Table 8), and as with the phosphodiester BDNPP (Table 7) the activity is even higher than with the diferric complex (see above). The main reason is a significantly lower affinity of the divalent site for substrate coordination.

CONCLUSION

The heterovalent $[Fe^{III}Fe^{II}(L^3)(OH)(OH_2)_2]^{3+}$ complex was designed to stabilize monodentate coordination of phosphomonoester substrates at the divalent site of the dinuclear complex, enabling nucleophilic attack by a terminal hydroxo

dx.doi.org/10.1021/ic301347t | Inorg. Chem. 2012, 51, 12195–12209

Table 7. Kinetic Parameters for BDNPP Hydrolysis with $[Fe^{III}_2(H_2L^2)(OH)]^{4+}$, $[Fe^{III}_2(L^3)(OH)(OH_2)_2]^{4+}$, and $[Fe^{III}Fe^{II}(L^3)(OH)(OH_2)_2]^{3+}$ in Comparison to the Diferric Complex of HL[1]

catalyst	pH_{max}	pK_a(I)	pK_a(II)	$10^4\ k_{cat}$ [s^{-1}]	K_M [mM]	k_{cat}/K_M [$M^{-1}\ s^{-1}$] × 10^{-2}
Fe^{III}_2/L^2	6.45	5.16 ± 0.10	7.43 ± 0.11	4.67 ± 0.26	5.92 ± 0.62	7.89 ± 0.09
Fe^{III}_2/L^3	7.44	5.39 ± 0.03	9.38 ± 0.10	6.48 ± 0.34	7.38 ± 0.69	8.79 ± 0.12
$Fe^{III}Fe^{II}/L^3$	6.69	5.30 ± 0.06	8.02 ± 0.19	11.4 ± 0.36	2.30 ± 0.24	49.6 ± 1.1
Fe^{III}_2/L^1	6.35	5.00 ± 0.11	7.15 ± 0.14	1.69 ± 0.14	1.74 ± 0.35	9.71 ± 0.08

Table 8. Kinetic Parameters for DNPP Hydrolysis with $[Fe^{III}_2(H_2L^3)(OH)_3]^{4+}$ and $[Fe^{III}Fe^{II}(L^3)(OH)(OH_2)_2]^{3+}$

catalyst	pH_{max}	pK_a(I)	pK_a(II)	$10^4\ k_{cat}$ [s^{-1}]	K_M [μM]	k_{cat}/K_M [$M^{-1}\ s^{-1}$]
Fe^{III}_2/L^3	6.95	5.17 ± 0.12	8.32 ± 0.59	1.33 ± 0.08	9.73 ± 0.05	13.6 ± 1.4
$Fe^{III}Fe^{II}/L^3$	6.91	5.79 ± 0.20	8.03 ± 0.10	2.34 ± 0.17	7.93 ± 2.89	29.5 ± 1.6

group at the trivalent site. Through a kinetic study, we demonstrated that we successfully characterized the first heterovalent monoesterase model system which provides further evidence for the widely accepted mechanism of phosphoester hydrolysis by PAPs.[2,3] Interestingly, the catalytic efficiency of the heterovalent catalyst is significantly higher, both for mono- and for diesterase activity, and this may be a reason why nature uses $Fe^{III}M^{II}$ active sites in PAP enzymes. Admittedly, the structural evidence for $[Fe^{III}Fe^{II}(L^3)(OH)(OH_2)_2]^{3+}$ is to some extent circumstantial[39] but supported by a thorough spectroscopic analysis (involving electronic, IR, EPR, NMR, and Mössbauer spectroscopies) and the observed reactivities.

EXPERIMENTAL SECTION

Analytical Methods. NMR spectra were recorded at 399.89 (^{1}H), 100.55 (^{13}C), and 161.88 MHz (^{31}P) with a Bruker Avance II 400 instrument. For ^{1}H and ^{13}C spectra the respective solvent peak and for ^{31}P spectra 85% H_3PO_4 (0 ppm) was used as reference for the chemical shift δ. All reported coupling constants ^nJ are for ^{1}H−^{1}H couplings. The following abbreviations are used for signal multiplicities: s = singlet, bs = broad singlet, d = doublet, t = triplet, q = quartet, quin = quintet, dd = doublet of doublets, ddd = doublet of doublets of doublets, dt = doublet of triplets, tt = triplet of triplets, m = multiplet. IR measurements were performed with a Perkin-Elmer 16 PC FT-IR spectrometer in KBr. Signal intensities are abbreviated as followed: b = broad, w = weak, m = medium, s = strong. UV−vis spectra and time-course measurements at fixed wavelengths were recorded with a JASCO V-570 spectrophotometer equipped with a JASCO ETC-505T cryostat at 25 °C. Time-dependent UV−vis measurements were performed using a TIDAS II J&M spectrophotometer. The baseline was recorded prior to a measurement series using pure solvent and subtracted automatically. Elemental analyses were performed in the analytical laboratories of the Chemical Institutes at the University of Heidelberg with an Elementar Vario EL machine. FAB mass spectra were measured with a Finnigan TSQ 700 instrument with nitrobenzylalcohol as the matrix at the Institute of Inorganic Chemistry at the University of Heidelberg. ESI mass spectra were measured with a Micromass Q-TOF Ultima spectrometer at the Institute of Inorganic Chemistry at the University of Heidelberg. HR-ESI mass spectra were measured with a Bruker Apex-Qe hybrid 9.4 T FT-ICR instrument at the Institute of Organic Chemistry at the University of Heidelberg. CV measurements were performed with a CH Instruments CHI660D electrochemical workstation equipped with a Faraday cage using a three-electrode setup consisting of a glassy carbon working electrode, a platinum wire as counter electrode, and a Ag/Ag^+ (0.1 mM in MeCN) reference electrode. Samples were prepared in degassed solvents with 0.1 M NBu_4ClO_4 as electrolyte. Redox potentials of the obtained signals were determined by comparison to a $FeCp_2$ sample measured at the same conditions and referenced vs SCE. pH values of the buffer solutions were adjusted at 25 °C with a Metrohm 713 pH meter equipped with a KCl electrode and calibrated with pH standard solutions at pH 4, 7, and 9.

Synthesis of H_3L^2 and HL^3. *N-(6-Pivaloylamido-2-pyridylmethyl)-N-(2-pyridylmethyl)amine.* 2-Formyl-6-pivaloylamido-pyridine (**1**) (2.20 g, 10.70 mmol) and picolylamine (1.27 g, 11.70 mmol) were dissolved in MeOH (45 mL) and stirred for 2.5 h at ambient temperature (rt). The solution was cooled to 0 °C, and $NaBH_4$ (0.44 g, 11.70 mmol) was added in small portions. The mixture was stirred overnight, H_2O (45 mL) was added, and the MeOH was removed in vacuo. Aqueous phase was extracted with ethyl acetate (3 × 70 mL), the organic phase was dried over Na_2SO_4, and the solvent was removed in vacuo to give *N*-(6-pivaloylamido-2-pyridylmethyl)-*N*-(2-pyridylmethyl)amine (**2**) as a yellow oil (3.52 g, 100%). ^{1}H NMR (300 MHz, $CDCl_3$): δ = 8.54 (d, $^3J_{H,H}$ = 4.8 Hz, 1H, N−CH_{ar}), 8.10 (d, $^3J_{H,H}$ = 8.0 Hz, 1H, CH_{ar}), 7.68−7.56 (m, 2H, CH_{ar}), 7.34 (d, $^3J_{H,H}$ = 7.8 Hz, 1H, CH_{ar}), 7.10−7.20 (m, 1H, CH_{ar}), 7.01 (d, $^3J_{H,H}$ = 7.4 Hz, 1H, CH_{ar}), 4.00 (s, 2H, CH_2), 3.90 (s, 2H, CH_2), 3.50 (bs, 1H, NH_{aliph}), 1.31 (s, 9H, C(CH_3)$_3$). ^{13}C NMR (100 MHz, $CDCl_3$): δ = 177.1 (C═O), 158.4, 156.6, 151.2 ($C_{q,ar}$), 149.2, 138.8, 136.6, 122.5, 122.2, 118.0, 112.1 (CH_{ar}), 54.2, 53.7 (CH_2), 39.7 (C(CH_3)$_3$), 27.4 (C(CH_3)$_3$). FAB$^+$-MS (nibeol) *m*/*z* (%): 299.2 (100) $[M + H]^+$.

N-(6-Amino-2-pyridylmethyl)-N-(2-pyridylmethyl)amine. N-(6-Pivaloylamido-2-pyridylmethyl)-*N*-(2-pyridylmethyl)amine (**2**) (1.80 g, 6.00 mmol) was refluxed in 2 M HCl (75 mL) for 48 h. After cooling to rt, 1 M NaOH solution was added until the pH reached 14. After extraction with dichloromethane (DCM, 3 × 200 mL), the organic phase was dried over Na_2SO_4 and the solvent was removed in vacuo to give *N*-(6-amino-2-pyridylmethyl)-*N*-(2-pyridylmethyl)amine (**3**) as a yellow oil (1.29 g, 100%). ^{1}H NMR (400 MHz, MeOH-d_4): δ = 8.55 (d, $^3J_{H,H}$ = 4.8 Hz, 1H, N−CH_{ar}), 7.82 (dt, $^3J_{H,H}$ = 7.8 Hz, $^4J_{H,H}$ = 1.6 Hz, 1H, CH_{ar}), 7.50−7.30 (m, 3H, CH_{ar}), 6.61 (d, $^3J_{H,H}$ = 7.2 Hz, 1H, CH_{ar}), 6.49 (d, $^3J_{H,H}$ = 8.2 Hz, 1H, arom. H), 4.12 (s, 2H, CH_2), 3.91 (s, 2H, CH_2). ^{13}C NMR (100 MHz, $CDCl_3$): δ = 161.0, 157.0, 154.3 ($C_{q,ar}$), 150.2, 139.8, 138.7, 124.3, 124.2, 112.4, 109.2 (CH_{ar}), 53.4 (2×) (CH_2). FAB$^+$-MS (nibeol) *m*/*z* (%): 215.2 (100) $[M + H]^+$.

N,N′-(6,6′-((((2-Hydroxy-5-methyl-1,3-phenylene)bis(methylene)-bis((pyridin-2-ylmethyl)azanediyl))bis(methylene))bis(pyridine-6,2-diyl))bis(2,2-dimethylpropanamide) (H_3L^2). 2,6-Bis(chloromethyl)-*p*-cresol (1.03 g, 5.00 mmol) was dissolved in DCM (8 mL) and cooled to 0 °C. *N*-(6-Pivaloylamido-2-pyridylmethyl)-*N*-(2-pyridylmethyl)-amine (**2**) (2.98 g, 10.00 mmol) and triethylamine (1.01 g, 10.00 mmol) were dissolved in THF (9 mL) and added dropwise. The solution was stirred at rt for 2 days and then filtered, and the solvents were removed in vacuo. The residue was dissolved in DCM (75 mL), washed with brine, dried over Na_2SO_4, and the solvent was removed in vacuo to give H_3L^2 as a pale-brown foam (3.64 g, 100%). ^{1}H NMR (500 MHz, $CDCl_3$): δ = 8.48 (d, $^3J_{H,H}$ = 4.1 Hz, 2H, CH_{py}−N), 8.25 (bs, 2H, NH), 8.08 (d, $^3J_{H,H}$ = 9.0 Hz, 2H, HNC$_q$−CH_{py}), 7.61 (t, $^3J_{H,H}$ = 7.8 Hz, 2H, para to N), 7.56 (dt, $^3J_{H,H}$ = 7.6 Hz, $^4J_{H,H}$ = 1.8 Hz, 2H, CH_{py} para to N), 7.48 (d, $^3J_{H,H}$ = 7.8 Hz, 2H, CH_{py}), 7.14−7.06 (m, 4H, CH_{py}), 7.05 (s, 2H, CH_{phenol}), 3.86 (s, 4H, CH_2), 3.80 (s, 4H, CH_2), 3.77 (s, 4H, CH_2), 2.26 (s, 3H, phenol−CH_3), 1.31 (s, 18H, C(CH_3)$_3$). ^{13}C NMR (125 MHz, $CDCl_3$): δ = 177.2 (NH−C═O),

dx.doi.org/10.1021/ic301347t | Inorg. Chem. 2012, 51, 12195−12209

155.5 ($C_{q,py}$), 153.1 ($C_{q,py}$), 151.1 (C_q–OH), 148.8 (CH_{py}–N), 148.7 (C_q–NH), 138.9, 136.7 (CH_{py}), 136.6 (C_q–CH_3), 130.0 (CH_{phenol}), 127.8 (C_q–CH_2), 123.0, 122.0, 117.9, 111.8 (CH_{py}), 59.8, 58.7 (N–CH_2-py), 54.8 (N–CH_2-phenol), 39.8 ($C(CH_3)_3$), 28.0 ($C(CH_3)_3$), 20.6 (CH_3). FAB$^+$-MS (nibeol) m/z (%): 729.4 (100) $[M + H]^+$. IR (KBr): $\tilde{\nu}$ [cm^{-1}] = 3559 (b), 3396 (w) 3065 (w), 2964 (m), 2929 (m), 2870 (m), 2821 (m), 1690 (s), 1596 (s), 1578 (s), 1523 (s), 1478 (s), 1455 (s), 1403 (m), 1367 (m), 1304 (s), 1224 (m), 1152 (m), 1125 (w), 1082 (w), 996 (m), 861 (w), 799 (m), 760 (m), 623 (w), 577 (w). Anal. Calcd for $C_{43}H_{52}N_8O_3$·0.33DCM: C, 68.73; H, 7.01; N, 14.80. Found: C, 68.69; H, 7.07; N, 14.56.

2,6-Bis((((6-aminopyridin-2-yl)methyl)(pyridin-2-ylmethyl)-amino)methyl)-4-methylphenol (HL^3). 2,6-Bis(chloromethyl)-*p*-cresol (0.62 g, 3.00 mmol) was dissolved in DCM (5 mL) and cooled to 0 °C. *N*-(6-Amino-2-pyridylmethyl)-*N*-(2-pyridylmethyl)amine (**3**) (1.29 g, 6.00 mmol) and triethylamine (0.61 g, 6.00 mmol) were dissolved in THF (6 mL) and added dropwise. The solution was stirred at rt for 2 days and filtered, and solvents were removed in vacuo. The residue was dissolved in DCM (50 mL), washed with brine, and dried over Na_2SO_4, and the solvent was removed in vacuo to give HL^3 as a pale-brown foam (1.62 g, 96%). ^{1}H NMR (500 MHz, $CDCl_3$): δ = 8.47 (d, $^3J_{H,H}$ = 4.4 Hz, 2H, CH_{py}–N), 7.56 (t, $^3J_{H,H}$ = 8.2 Hz, 2H, CH_{py} para to N), 7.35 (t, $^3J_{H,H}$ = 7.8 Hz, 2H, CH_{py} para to N), 7.08 (m, 4H, CH_{py}), 6.97 (s, 2H, CH_{phenol}), 6.78 (d, 2H, $^3J_{H,H}$ = 7.2 Hz, NH_2C_q–CH_{py}), 6.34 (d, 2H, $^3J_{H,H}$ = 8.0 Hz, CH_{py}), 4.50 (bs, 4H, NH_2), 3.84 (s, 4H, CH_2), 3.74 (s, 4H, CH_2), 3.69 (s, 4H, CH_2), 2.22 (s, 3H, CH_3). ^{13}C NMR (125 MHz, $CDCl_3$): δ = 159.2 (C_q–NH_2), 157.9, 153.5 ($C_{q,py}$), 149.1 (C_q–OH), 148.6 (CH_{py}–N), 138.5, 136.5, 130.1 (CH_{phenol}), 127.2 (C_q–CH_3), 123.0 (CH_{py}), 122.4 (C_q–CH_2), 121.9, 112.5, 107.2 (CH_{py}), 59.7, 58.9 (N–CH_2-py), 55.0 (N–CH_2-phenol), 20.6 (CH_3). FAB$^+$-MS (nibeol) m/z (%): 561.3 (100) $[M + H]^+$. *IR* (KBr): $\tilde{\nu}$ [cm^{-1}] = 3454 (b), 3380 (b), 3342 (b), 3187 (w), 2915 (w), 2814 (w), 1615 (s), 1594 (s), 1571 (s), 1465 (s), 1434 (s), 1361 (m), 1298 (m), 1229 (m), 1159 (w), 1119 (w), 1092 (w), 1045 (w), 996 (m), 864 (w), 790 (m), 760 (m). Anal. Calcd for $C_{33}H_{36}N_8O$·0.33DCM: C, 67.97; H, 6.27; N, 19.02. Found: C, 68.11; H, 6.28; N, 17.51.

Synthesis of $[Fe^{III}_2(H_2L^2)(OH)](ClO_4)_4$·$CH_3OH$. Ligand H_3L^2 (110 mg, 0.15 mmol) was dissolved in 10 mL of MeOH and heated to 50 °C. Ferric perchlorate hydrate (100 mg, 0.30 mmol) was added in 2 mL of MeOH while stirring. The solution immediately turned dark green and was heated at 50 °C for 1 h. The complex was precipitated by diffusion of diethyl ether into solution. Product was filtered off and dried in vacuo to yield $[Fe^{III}_2(H_2L^2)(OH)]^{4+}$ as a very dark green powder (0.13 g, 69%). HR-ESI$^+$-MS (MeOH) m/z (%): 882.29171 (calcd 882.29187) (100) $[(H_2L^2)Fe^{III}(ClO_4)]^+$; 896.32903 (calcd 896.32843) (49) $[Na(H_2L^2)Fe^{III}(HCO_2)_2]^+$; 934.22315 (calcd 934.22220) (38) $[LFe^{III}_2SO_4]^+$. UV–vis (MeCN): λ_{max} [nm] (ε [M^{-1} cm^{-1}]) = 228 (sh) (32 473), 258 (sh) (20 290), 284 (17 562), 361 (sh) (4134), 685 (1946). IR (KBr): $\tilde{\nu}$ [cm^{-1}] = 3430 (b), 3085 (w), 2975 (w), 2936 (w), 2875 (w), 2016 (w), 1679 (w), 1624 (s), 1608 (s), 1573 (w), 1528 (m), 1463 (m), 1431 (m), 1371 (w), 1263 (w), 1143 (s); 1111 (s), 1089 (s), 1023 (m), 922 (w), 809 (w), 767 (w), 636 (m), 626 (m). Anal. Calcd for $C_{43}H_{52}N_8O_{20}Fe_2Cl_4$·MeOH: C, 41.08; H, 4.39; N, 8.71. Found: C, 41.78; H, 4.86; N, 8.71.

Synthesis of $[Fe^{III}_2(L^3)(OH)(OH_2)_2]^+(ClO_4)_4$·0.5MeCN·$Et_2O$. Ligand HL^3 (200 mg, 0.35 mmol) was dissolved in 50 mL of MeOH and heated to 50 °C. Ferric perchlorate hydrate (250 mg, 0.70 mmol) was added in 5 mL of MeOH while stirring. The solution immediately turned dark blue and was heated at 50 °C for 1 h. The solvent was removed in vacuo, and the residue was taken up in a small volume of MeCN. The complex was precipitated by diffusion of diethyl ether into solution. Product was filtered off and dried in vacuo to yield $[Fe^{III}_2(L^3)(OH)(OH_2)_2]^{4+}$ as a very dark blue powder (0.29 g, 77%). HR-ESI$^+$-MS (MeOH): not detectable. UV–vis (MeCN): λ_{max} [nm] (ε [M^{-1} cm^{-1}]) = 232 (28 065), 256 (sh) (19 297), 302 (16 044), 365 (sh) (4374), 590 (2238). IR (KBr): $\tilde{\nu}$ [cm^{-1}] = 3370 (b), 3201 (b), 3094 (w), 2940 (w), 2865 (w), 2022 (w), 1661 (s), 1634 (s), 1572 (m), 1480 (m), 1445 (m), 1298 (w), 1265 (w), 1144 (s), 1111 (s), 1088 (s), 1025 (w), 1008 (w), 855 (w), 802 (m), 763 (m), 636 (m), 627 (m). Anal. Calcd for $C_{33}H_{40}N_8Cl_4Fe_2O_{20}$·0.5MeCN·$Et_2O$: C, 38.19; H, 4.37; N, 9.97. Found: C, 38.47; H, 4.25; N, 9.97.

Electrochemical Reduction of $[Fe^{III}_2(H_2L^2)(OH)]^{4+}$ and $[Fe^{III}_2(L^3)-(OH)(OH_2)_2]^{4+}$. The electrochemical reduction of $[Fe^{III}_2(H_2L^2)-(OH)]^{4+}$ and $[Fe^{III}_2(L^3)(OH)(OH_2)_2]^{4+}$ was performed by bulk electrolysis using a CH Instruments CHI660D electrochemical workstation with a graphite sponge as working electrode, a platinum wire as counter electrode, and a Ag/Ag$^+$ (0.1 mM in MeCN) reference electrode. Complexes were prepared in situ by dissolving the ligand (1 mM) and ferric salt (2 mM) in degassed and pre-electrolyzed MeCN (30 min at −200 mV; I = 0.1 M NBu_4ClO_4) and stirring for 5 min. Potential was kept at −200 mV until the current reached a plateau. A total charge transfer of 1 eq electrons was observed. Electrolyzed solutions were kept under argon.

Synthesis of the ^{57}Fe-Enriched Complex $[^{57}Fe^{III}_2(H_2L^2)(OH)]^{4+}$. ^{57}Fe-enriched metallic iron (95% enrichment, 38 mg, 0.66 mmol) was heated in conc. HCl (50 mL) at 120 °C for 24 h. Solvent was removed in vacuo, and the resulting yellow residue of crude $^{57}FeCl_3$ was dissolved in ethanol (5 mL). Tetraethylammonium chloride (110 mg, 0.66 mmol) was added while stirring, and the bright yellow precipitate of $(NEt_4)[^{57}FeCl_4]$ was collected, washed with cold ethanol, and dried in vacuo. HR-ESI$^-$-MS (MeOH): 198.80833 (calcd 198.80786) (100) $[^{57}FeCl_4]^-$. Anal. Calcd for $C_8H_{20}NCl_4{}^{57}Fe$: C, 29.21; H, 6.13; N, 4.26. Found: C, 29.22; H, 6.10; N, 4.34. H_3L^2 (36.4 mg, 0.05 mmol) was dissolved in pre-electrolyzed MeCN (50 mL, with 0.1 M NBu_4ClO_4), and $(NEt_4)[^{57}FeCl_4]$ (32.9 mg, 0.1 mmol) was added while stirring. For Mössbauer measurements the resulting 1 mM solution was electrolyzed at −200 mV until the current reached a plateau. A total charge transfer of less than 1 eq electrons was observed (around 0.5 equiv); this is probably due to the high complex concentration required for the Mössbauer experiment (overloaded working electrode).

EPR Spectroscopy. Variable-temperature (1.8–16 K) X-band EPR spectra (ca. 9 GHz) were recorded with a Bruker Biospin ELEXSYS E580 spectrometer equipped with a Super High Q cavity and an Oxford Instruments ESR 910 cryostat in conjunction with an Oxford Instruments ITC503 temperature controller, located at the Centre for Advanced Imaging at the University of Queensland, Australia. The microwave frequency and magnetic field were calibrated with a Bruker frequency counter and an ER036 TM Tesla meter. At higher temperatures (130 and 298 K) X-band EPR spectra (ca. 9 GHz) were recorded with a Bruker Biospin ELEXSYS E500 spectrometer with a Super High Q cavity located at the Institute of Inorganic Chemistry (University Heidelberg). For measurements at 130 K, a Eurotherm temperature controller in conjunction with a liquid nitrogen flow-through system was used. Spin Hamiltonian parameters for the dinuclear iron complexes and radical species were determined from computer simulation of the experimental spectra using MoSophe and the XSophe–Sophe-XeprView computer simulation suites, respectively.[48,49] Simulated and experimental spectra were visualized with Xepr.

Mössbauer Spectroscopy. ^{57}Fe Mössbauer spectra of frozen solutions were acquired using a conventional spectrometer in the constant-acceleration mode equipped with a ^{57}Co source (3.7 GBq) in a rhodium matrix. Isomer shifts are given relative to α-Fe at room temperature. Frozen samples were inserted into an Oxford Instruments Mössbauer-Spectromag 4000 Cryostat, which has a split-pair superconducting magnet system for applied fields up to 5 T (not used in the experiments described here), with the field of the sample oriented perpendicular to the γ-ray direction, while the sample temperature can be varied between 3.0 and 300 K.

Kinetic Measurements of BDNPP and DNPP Hydrolysis. Phosphatase activity for the activated diester substrate bisdinitrophenylphosphate (BDNPP) was determined in acetonitrile/buffer (1:1) at 25 °C between pH 4.6 and 10. pH values reported refer to the aqueous component, i.e., these are "apparent pH values". We note that the pH meter reading of a solution of the buffer was the same within error as that of a 1:1 mixture of buffer and acetonitrile,[2,3,42,65] i.e., the values reported here are well suited for comparison with other catalysts). Product formation (2,4-dinitrophenolate) was observed spectrophoto-

metrically at 400 nm. To obtain the starting activity, the time between 30 and 240 s was analyzed by linear regression. A multicomponent buffer was used containing MES, HEPES, and CHES (all 50 mM) and $LiClO_4$ (250 mM) in Milli-Q water. The desired pH was adjusted with aq. NaOH. Complex and substrate solutions were prepared separately in MeCN, and their final concentrations in the cuvette were 0.04 and 5 mM, respectively. This was varied for complex- and substrate-dependent measurements. Substrate-dependent data were fitted using the Michaelis–Menten equation, eq 1. pH profiles were fitted in Origin 8.1G using eq 2 for a diprotic system with two active species

$$v_0 = v_{0,\max}\frac{\left(1 + \frac{\gamma K_a(II)}{[H^+]}\right)}{\left(1 + \frac{[H^+]}{K_a(I)} + \frac{K_a(II)}{[H^+]}\right)} \quad (2)$$

$$k_{cat} = v_{max}/[K]_0 \quad (3)$$

where v and v_{max} are the initial and limiting rates, respectively, γ is the relative activity of the species in a given pH range, K_a are the kinetically relevant ionization constants, and $[K]$ is the complex concentration.[62,68] Phosphatase activity for the activated monoester substrate dinitrophenylphosphate (DNPP) was determined using a similar approach as for the BDNPP assays with the following alterations: DNPP was dissolved in buffer of the desired pH. The final concentration in the cuvette was 0.5 mM. Autohydrolysis rates were determined prior to as well as directly after the two catalytic measurements for each pH. Spectral changes that affected the rates due to ligand exchange at the complex were also recorded and subtracted at the end.

DFT Calculations. DFT geometry optimizations were performed with Gaussian 09,[69] with the B3LYP functional,[70,71] the TZVP basis set for Fe and P, and the SVP basis set for C, H, N, and O.[72,73] Optimized structures were confirmed by frequency calculations as minima on the potential energy surface, and reported energies are zero-point corrected. J values, g values, and zero-field splitting tensors[74] of the geometry-optimized complexes were calculated with Orca 2.6, rev.04[75,76] with the same functional and basis set as before, except using TZVP on O instead of SVP.[72,73] J values were calculated using the broken symmetry method implemented in Orca.[77]

■ ASSOCIATED CONTENT

Ⓢ Supporting Information

Time-dependent UV–vis spectra of the heterovalent complexes under aerobic conditions, all pH profiles and Michaelis–Menten analyses with BDNPP and DNPP as substrate and both catalysts (diferric and heterovalent forms), overlay plots of the species distributions with the kinetic profiles, and EPR spectra of the ^{57}Fe-labeled sample. This material is available free of charge via the Internet at http://pubs.acs.org.

■ AUTHOR INFORMATION

Corresponding Author

*Fax: +49-6221-546617. E-mail: peter.comba@aci.uni-heidelberg.de.

Notes

The authors declare no competing financial interest.

■ ACKNOWLEDGMENTS

Financial support by the German Science Foundation (DFG), the German Academic Exchange Service (DAAD), the University of Heidelberg, and the University of Queensland are gratefully acknowledged.

■ REFERENCES

(1) Wilcox, D. E. *Chem. Rev.* **1996**, *96*, 2435.
(2) Mitić, N.; Smith, S. J.; Neves, A.; Guddat, L. W.; Gahan, L. R.; Schenk, G. *Chem. Rev.* **2006**, *106*, 3338.
(3) Schenk, G.; Mitić, N.; Hanson, G.; Comba, P. *Coord. Chem. Rev.* **2012**, in press.
(4) Krauss, M. *J. Chem. Inf. Comput. Sci.* **2001**, *41*, 8.
(5) Zheng, F.; Zhan, C.-G.; Ornstein, R. L. *J. Phys. Chem. B* **2002**, *106*, 717.
(6) Ferreira, D. E. C.; De Almeida, W. B.; Neves, A.; Rocha, W. R. *Phys. Chem. Chem. Phys.* **2008**, *10*, 7039.
(7) Alberto, M. E.; Marino, T.; Ramos, M. J.; Russo, N. *J. Chem. Theory Comput.* **2010**, *6*, 2424.
(8) Than, R.; Feldmann, A. A.; Krebs, B. *Coord. Chem. Rev.* **1999**, *182*, 211.
(9) Xavier, F. R.; Neves, A.; Casellato, A.; Peralta, R. A.; Bortoluzzi, A. J.; Szpoganicz, B.; Severino, P. C.; Terenzi, H.; Tomkowicz, Z.; Ostrovsky, S.; Haase, W.; Ozarowski, A.; Krzystek, J.; Telser, J.; Schenk, G.; Gahan, L. R. *Inorg. Chem.* **2009**, *48*, 7905.
(10) Schenk, G.; Peralta, R. A.; Batista, S. C.; Bortoluzzi, A. J.; Szpoganicz, B.; Dick, A.; Herrald, P.; Hanson, G. R.; Szilagyi, R. K.; Riley, M. J.; Gahan, L. R.; Neves, A. *J. Biol. Inorg. Chem.* **2008**, *13*, 139.
(11) Boudalis, A. K.; Aston, R.; Smith, S. J.; Mirams, R.; Riley, M. J.; Schenk, G.; Blackman, A. G.; Hanton, L. R.; Gahan, L. R. *J. Chem. Soc., Dalton Trans.* **2007**, 5132.
(12) Lanznaster, M.; Neves, A.; Bortoluzzi, A. J.; Aires, V. V. E.; Szpoganicz, B.; Terenzi, H.; Severino, P. C.; Fuller, J. M.; Drew, S. C.; Gahan, L. R.; Hanson, G. R.; Riley, M. J.; Schenk, G. *J. Biol. Inorg. Chem.* **2005**, *10*, 319.
(13) Mitić, N.; Noble, C. J.; Gahan, L. R.; Hanson, G. R.; Schenk, G. *J. Am. Chem. Soc.* **2009**, *131*, 8173.
(14) Daumann, L. J.; Gahan, L. R.; Comba, P.; Schenk, G. *Inorg. Chem.* **2012**, *51*, 7669.
(15) Comba, P.; Gahan, L. R.; Hanson, G. R.; Mereacre, V.; Noble, C. J.; Powell, A. K.; Prisecaru, I.; Schenk, G.; Zajaczkowski-Fischer, M. *Chem.—Eur. J.* **2012**, *18*, 1700.
(16) Comba, P.; Gahan, L. R.; Hanson, G. R.; Westphal, M. *Chem. Commun.* **2012**, 9364.
(17) Klabunde, T.; Strater, N.; Frohlich, R.; Witzel, H.; Krebs, B. *J. Mol. Biol.* **1996**, *259*, 737.
(18) Dietrich, M.; Münstermann, D.; Suerbaum, H.; Witzel, H. *Eur. J. Biochem.* **1991**, *199*, 105.
(19) Schenk, G.; Elliott, T. W.; Leung, E.; Carrington, L. E.; Mitić, N.; Gahan, L. R.; Guddat, L. W. *BMC Struct. Biol.* **2008**, *8*, 6.
(20) Mitić, N.; Hadler, K. S.; Gahan, L. R.; Hengge, A. C.; Schenk, G. *J. Am. Chem. Soc.* **2010**, *132*, 7049.
(21) Schepers, K.; Bremer, B.; Krebs, B.; Henkel, G.; Althaus, E.; Mosel, B.; Müller-Warmuth, W. *Angew. Chem., Int. Ed. Engl.* **1990**, *29*, 531.
(22) Neves, A.; deBrito, M. A.; Vencato, I.; Drago, V.; Griesar, K.; Haase, W. *Inorg. Chem.* **1996**, *35*, 2360.
(23) Gahan, L. R.; Smith, S. J.; Neves, A.; Schenk, G. *Eur. J. Inorg. Chem.* **2009**, 2745.
(24) Kaljurand, I.; Kutt, A.; Soovali, L.; Rodima, T.; Maemets, V.; Leito, I.; Koppel, I. *J. Org. Chem.* **2005**, *70*, 1019.
(25) Feng, G.; Mareque-Rivas, J. C.; Martin de Rosales, T. R.; Williams, N. H. *J. Am. Chem. Soc.* **2005**, *127*, 13470.
(26) Feng, G.; Natale, D.; Prabaharan, R.; Mareque-Rivas, J. C.; Williams, N. H. *Angew. Chem., Int. Ed.* **2006**, *45*, 7056.
(27) Feng, G.; Mareque-Rivas, J. C.; Williams, N. H. *Chem. Commun.* **2006**, 1845.
(28) Linjalahti, H.; Feng, G.; Mareque-Rivas, J. C.; Mikkola, S.; Williams, N. H. *J. Am. Chem. Soc.* **2008**, *130*, 4232.
(29) An asymmetric ligand with two different cavities obviously would have been more attractive but more difficult to synthesize; we therefore prepared and studied H_3L^2 and HL^3 in the present study to test the general concept.
(30) Suzuki, M.; Kanatomi, H.; Murase, I. *Chem. Lett.* **1981**, 1745.
(31) Borovik, A. S.; Papaefthymiou, V.; Taylor, L. F.; Anderson, O. P.; Que, L. *J. Am. Chem. Soc.* **1989**, *111*, 6183.
(32) Borovik, A. S.; Que, L. *J. Am. Chem. Soc.* **1988**, *110*, 2345.

(33) Inomata, T.; Shinozaki, K.; Hayashi, Y.; Arii, H.; Funahashi, Y.; Ozawa, T.; Masuda, H. *Chem. Commun.* **2008**, 392.
(34) Tan, Y. C.; Gan, X. M.; Stanchfield, J. L.; Duesler, E. N.; Paine, R. T. *Inorg. Chem.* **2001**, *40*, 2910.
(35) Liu, Q.; Rovis, T. *J. Am. Chem. Soc.* **2006**, *128*, 2552.
(36) MacroModel[37] in Maestro 8.5.111; torsional sampling (Monte Carlo multiple minimum search) with 1000 steps produced 50−200 different structures which were geometry optimized in up to 50 000 iterations [MM3*],[38] steepest descent, gradient convergence threshold 0.01.
(37) *MacroModel*, version 9.6; Schrödinger: New York, 2005.
(38) Allinger, N. L.; Yuh, Y. H.; Lii, J.-H. *J. Am. Chem. Soc.* **1989**, *111*, 8551.
(39) These stoichiometric formula for the diferric complexes (analoguous stoichiometries are derived for the heterovalent systems) are used throughout; these are derived from elemental analyses and mass spectrometry and are fully reproducible. The structural proposals (see, e.g., Chart 2) emerge from these stoichiometries, spectroscopic measurements, spectrophotometric pH titrations, structural analyses of similar systems,[2,14,40,41] and the proposed catalytic mechanism. Note that the amine-based ligand complex $[Fe^{III}_2(L^3)(OH)(OH_2)_2]^{4+}$ may also be formulated as a tautomer with two terminal hydroxides and two ammonium pendents. This however is unlikely due to the corresponding pK_a values and the reactivity profile, i.e., as usual, at higher pH the reactivity decreases since the exchange of phosphoesters with hydroxides is slow.
(40) Neves, A.; Lanznaster, M.; Bortoluzzi, A. J.; Peralta, R. A.; Casellato, A.; Castellano, E. E.; Herrald, P.; Riley, M. J.; Schenk, G. *J. Am. Chem. Soc.* **2007**, *129*, 7486.
(41) Ng, G. K.-Y.; Ziller, J. W.; Borovik, A. S. *Inorg. Chem.* **2011**, *50*, 7922.
(42) Smith, S. J.; Peralta, R. A.; Jovito, R.; Horn, J. A.; Bortoluzzi, A. J.; Noble, C. J.; Hanson, G. R.; Stranger, R.; Jayaratne, V.; Cavigliasso, G.; Gahan, L. R.; Schenk, G.; Nascimento, O. R.; Cavalett, A.; Bortolotto, T.; Razzera, G.; Terenzi, H.; Neves, A.; Riley, M. *Inorg. Chem.* **2012**, *51*, 2065.
(43) Kriss, G. A. In *Astronomical Data Analysis Software & Systems III*; Crabtree, D. R., Hanisch, R. J., Barnes, J., Ed.; Astronomical Society of the Pacific: San Francisco, 1994; Vol. *61*.
(44) Note that the CVs, under the conditions of the experiments described here, are unresolved and not fully reversible. Consequently, the potentials reported in Table 1 must be interpreted with some caution, that is, only the relative values (difference between the H_3L^2- and the HL^3-based systems) and the order of magnitude of the difference to other model systems are relevant in our general discussion.
(45) Note that for preparative reasons it is inevitable that the ^{57}Fe-labeled sample for Mössbauer spectroscopy may include some coordinated Cl^-.
(46) Evans, D. F. *J. Chem. Soc.* **1959**, 2003.
(47) Bernhardt, P. V.; Schenk, G.; Wilson, G. J. *Biochemistry* **2004**, *43*, 10387.
(48) Hanson, G. R.; Noble, C. J.; Benson, S. In *High Resolution EPR: Applications to Metalloenzymes and Metals in Medicine*; Hanson, G. R., Berliner, L. J., Eds.; 2009; Vol. *28*, p 105.
(49) Hanson, G. R.; Gates, K. E.; Noble, C. J.; Griffin, M.; Mitchell, A.; Benson, S. *J. Inorg. Biochem.* **2004**, *98*, 903.
(50) Superhyperfine coupling to two ^{57}Fe nuclei results in the splitting of each resonance into four, and the short half-life of the radical prevented measurement of a spectrum with a high signal-to-noise ratio. Attempts to use Fourier filtering or other filtering algorithms failed to yield a spectrum in which the S/N ratio of the weaker resonances at the edge of the spectrum was greater than 1:1. However, the additional splitting unambiguously proves that the radical is located on the ligand of the intact complex.
(51) Krebs, B.; Schepers, K.; Bremer, B.; Henkel, G.; Althaus, E.; Müller-Warmutz, W.; Griesar, K.; Haase, W. *Inorg. Chem.* **1907**, *33*, 1004.
(52) Nie, H. L.; Aubin, S. M. J.; Mashuta, M. S.; Wu, C. C.; Richardson, J. F.; Hendrickson, D. N.; Buchanan, R. M. *Inorg. Chem.* **1995**, *34*, 2382.
(53) Note also that, for practical reasons, the samples used for NMR spectroscopy contain Cl^-, similar to the Mössbauer samples but in difference to the samples for spectrophotometric titrations, EPR spectroscopy, electrochemistry, and mechanistic work, that is, Cl^- may also act as bridging ligand.
(54) Bunton, C. A.; Farber, S. J. *J. Org. Chem.* **1969**, *34*, 767.
(55) Rawji, G.; Milburn, R. M. *J. Org. Chem.* **1981**, *46*, 1205.
(56) Hope, D. B.; Horncastle, K. C. *J. Chem. Soc. C.* **1966**, 1098.
(57) Martin, A. E.; Ford, T. M.; Bulkowski, J. E. *J. Org. Chem.* **1982**, *47*, 412.
(58) Roelfes, G.; Vrajmasu, V.; Chen, K.; Ho, R. Y. N.; Rohde, J.; Zondervan, C.; la Crois, R. M.; Schudde, E. P.; Lutz, M.; Spek, A. L.; Hage, R.; Feringa, B.; Munck, E.; Que, L., Jr. *Inorg. Chem.* **2003**, *42*, 2639.
(59) Note that this procedure is the standard method in this field,[1−3,8] and this includes the solvents, model substrates, buffer systems, kinetic analysis, and experimental techniques, i.e., the results presented are largely comparable with other published data.
(60) Segel, I. H. *Enzyme kinetics: Behaviour and analysis of rapid equilibria and steady-state equilibria*; John Wiley and Sons: New York, 1993.
(61) Peralta, R.; Bortoluzzi, A. J.; de Souza, B.; Jovito, R.; Xavier, F. R.; Couto, R. A. A.; Casellato, A.; Nome, F.; Dick, A.; Gahan, L. R.; Schenk, G.; Hanson, G. R.; de Paula, F. C. S.; Pereira-Maia, E. C.; Machado, S.; Severino, P. C.; Pich, C.; Fischer, F. L.; Terenzi, H.; Castellano, E. E.; Neves, A.; Riley, M. J. *Inorg. Chem.* **2010**, *49*, 11421.
(62) Segel, I. H. *Enzyme Kinetics-Behavior and Analysis of Rapid Equilibrium and Steady-State Enzyme Systems*; Wiley-VCH: New York, 1975.
(63) Note that in the systems presented here, we do not have experimental evidence for monodentate coordination of the substrate, and this was shown unambiguously only in very few examples.[64]
(64) Daumann, L. J.; Dalle, K. E.; Schenk, G.; McGeary, R. P.; Bernhardt, P. V.; Ollis, D. L.; Gahan, L. R. *Dalton Trans.* **2012**, *41*, 1695.
(65) While obviously these values are not "true" pH values, for the present study, relative pH values are sufficient. Moreover, the procedure used here is standard in the field.[66,67]
(66) Kaminskaia, N. V.; He, C.; Lippard, S. J. *Inorg. Chem.* **2000**, *39*, 3365.
(67) Kaminskaia, N. V.; Spingler, B.; Lippard, S. J. *J. Am. Chem. Soc.* **2000**, *122*, 6411.
(68) Williams, R. J. P. In *Hematin Enzymes*; Falk, J. E., Lemberg, R., Morton, R. K., Eds.; Pergamon Press: Oxford, 1961; p 41.
(69) Frisch, M. J.; Trucks, G. W.; Schlegel, H. B.; Scuseria, G. E.; Robb, M. A.; Cheeseman, J. R.; Scalmani, G.; Barone, V.; Mennucci, B.; Petersson, G. A.; Nakatsuji, H.; Caricato, M.; Li, X.; Hratchian, H. P.; Izmaylov, A. F.; Bloino, J.; Zheng, G.; Sonnenberg, J. L.; Hada, M.; Ehara, M.; Toyota, K.; Fukuda, R.; Hasegawa, J.; Ishida, M.; Nakajima, T.; Honda, Y.; Kitao, O.; Nakai, H.; Vreven, T.; Montgomery Jr., J. A.; Peralta, J. E.; Ogliaro, F.; Bearpark, M.; Heyd, J. J.; Brothers, E.; Kudin, K. N.; Staroverov, V. N.; Kobayashi, R.; Normand, J.; Raghavachari, K.; Rendell, A.; Burant, J. C.; Iyengar, S.; Tomasi, J.; Cossi, M.; Rega, N.; Millam, N. J.; Klene, M.; Knox, J. E.; Cross, J. B.; Bakken, V.; Adamo, C.; Jaramillo, J.; Gomperts, R.; Stratmann, R. E.; Yazyev, O.; Austin, A. J.; Cammi, R.; Pomelli, C.; Ochterski, J. W.; Martin, R. L.; Morokuma, K.; Zakrzewski, V. G.; Voth, G. A.; Salvador, P.; Dannenberg, J. J.; Dapprich, S.; Daniels, A. D.; Farkas, O.; Foresman, J. B.; Ortiz, J. V.; Cioslowski, J.; Fox, D. J. *Gaussian 09*, Revision A.02, Gaussian, Inc.: Wallingford, CT, 2009.
(70) Becke, A. D. *Phys. Rev. A.* **1988**, *38*, 3098.
(71) Lee, C.; Yang, W.; Parr, R. G. *Phys. Rev. B* **1988**, *37*, 785.
(72) Schäfer, A.; Horn, H.; Ahlrichs, R. *J. Chem. Phys.* **1992**, *97*, 2571.
(73) Schäfer, A.; Huber, C.; Ahlrichs, R. *J. Chem. Phys.* **1994**, *100*, 5829.
(74) Neese, F.; Solomon, E. I. *Inorg. Chem.* **1998**, *37*, 6568.

(75) Neese, F. *J. Chem. Phys.* **2003**, *119*, 9428.
(76) Neese, F. *Int. J. Quantum Chem.* **2001**, *83*, 104.
(77) Neese, F. *J. Phys. Chem. Solids* **2004**, *65*, 781.